Ministry of Higher Education and Scientific Research

University of Babylon, College of Science

Department of Physics

Study of the Organic Dyes and Carbon Nanotubes for constructing Solar Cells Systems using First- Principle Calculations

A Thesis Submitted to the College of Science, University of Babylon in Partial Fulfillment of the Requirements for the Degree of Master of Science in Physics

BY

Noor Abdul Ameer Hameed Hussein

B.Sc. in Physics (2018)

Supervised by

Prof. Dr. Hayder M. Abduljali ***Assist. Prof. Dr. Hussein H. Abed***

2023 A.D **1444 A.H**

وزارة التعليم العالي والبحث العلمي

جامعة بابل / كلية العلوم

قسم الفيزياء

دراسة الصبغات العضوية وانابيب الكاربون النانوية لتشكيل انظمة خلايا شمسية باستعمال الحسابات الاولية

رسالة مقدمة الى قسم الفيزياء – كلية العلوم – جامعة بابل
وهي جزء من متطلبات نيل درجة الماجستير في علوم الفيزياء

من قبل

نور عبد الامير حميد حسين

بكالوريوس علوم فيزياء – جامعة بابل

(2018)

بإشراف

أ. د. حيدر محمد عبد الجليل ***أ. م. د. حسين حاكم عبد***

١٤٤٤هـ ٢٠٢٣ م

بِسْمِ اللهِ الرَّحْمنِ الرَّحِيمِ

۞ اللَّهُ نُورُ السَّمَاوَاتِ وَالْأَرْضِ ۚ مَثَلُ نُورِهِ كَمِشْكَاةٍ فِيهَا مِصْبَاحٌ ۖ الْمِصْبَاحُ فِي زُجَاجَةٍ ۖ الزُّجَاجَةُ كَأَنَّهَا كَوْكَبٌ دُرِّيٌّ يُوقَدُ مِن شَجَرَةٍ مُّبَارَكَةٍ زَيْتُونَةٍ لَّا شَرْقِيَّةٍ وَلَا غَرْبِيَّةٍ يَكَادُ زَيْتُهَا يُضِيءُ وَلَوْ لَمْ تَمْسَسْهُ نَارٌ ۚ نُّورٌ على نُورٍ ۗ يَهْدِي اللَّهُ لِنُورِهِ مَن يَشَاءُ ۚ وَيَضْرِبُ اللَّهُ الْأَمْثَالَ لِلنَّاسِ ۗ وَاللَّهُ بِكُلِّ شَيْءٍ عَلِيمٌ

صَدَقَ اللهُ العَلِيُّ العَظِيم

سورة النور الآية (٣٥)

Supervisor Certification

We certify that this thesis entitled (**Study of the Organic Dyes and Carbon Nanotubes for constructing Solar Cell Systems using First - Principle Calculations)** was prepared by (**Noor Abdul Ameer Hameed Hussein**) under our supervisions at Department of physics, College of Science, University of Babylon, as a partial fulfillment of the requirements for the Degree of Master of Science in Physics .

SUPERVISORS:

Signature : **Signature :**

Dr. Hayder M. Abduljalil **Dr. Hussein H. Abed**

Title : Prof. **Title :** Assist. Prof.

Address: Department of physics – College of science – University of Babylon.

Date : / /2023

Certification of the Head of the Department

In view of the available recommendation, I forward this thesis for debate by the examination committee.

Signature:

Name: Dr. Samira Adnan Mahdi

Title: Assist. Prof.

Address: Head of the Department of Physics - College of Science- University of Babylon

Date: / / 2023

Acknowledgments

At first, praise be to thank my God for His graces that enabled me to meet the requirements of my study and overcome the difficulties during the courses and research.

I would like to express my deep thanks and respect to Prof. Dr. Hayder M. AbdulJalil and Assist. Prof. Dr. Hussein Hakim Abed for their supervisions and for their efforts to accomplish my study.

I am grateful to Mohammed Ayad from the environmental recharge and study center, Babylon, Iraq for his help.

I would like to thank the center of recharging and environmental study and the Dean of college of sciences and the Head of Physics Department at the college of Science at University of Babylon.

Dedication

In the name of god …

And the holy Mohammed…

For the one who made me from the trash , For the soul of my precious mother …

To my supportive family and friends …

Noor

الخلاصة

تم فحص امكانية استخدام التراكيب النانوية لصبغة الازو النقية والمطعمة بذرات (Si, Ti, S, Zn, Al, Cu, Ni) كمتحسس للخلايا الشمسية الصبغية. استخدمت نظرية دالة الكثافة مع دالة الاساس 6-31G المدمجة مع الدالة الهجينة (B3LYP) لحساب الامثلية الهندسية للتراكيب النانوية وخواصها الالكترونية. درست امكانية التحسس للتراكيب النانوية ال (DSSCs) بواسطة المدار الجزيئي الاعلى المشغول (HOMO) والمدار الجزيئي الادنى الغير مشغول (LUMO) للتراكيب النانوية نسبة الى طاقة المحلول الالكتروليت $I^{`}/I_3^{`}$ وحزمة الطاقة الادنى لأقطاب (TiO_2) على التوالي وكذلك التوزيع الموضعي للشحنات بالإضافة الى فجوة الطاقة. تم استخدام دالة الكثافة المعتمدة على الزمن لحساب الامتصاص البصري و كفاءة الحصاد الضوئي للتراكيب النانوية قيد الدراسة.

النتائج اظهرت ان جميع التراكيب النانوية ماعدا صبغة الازو المطعمة بالألمنيوم تحقق متطلبات التحسس وان ثلاثة من النماذج الثمان المفترضة تحسن التوزيع الموضعي للشحنة .صبغة الازو المطعمة بذرة الكبريت بينت انها النظام الامثل للتحسس الشمسي لأفضل استقرار (LUMO) و (HOMO) واقل معدل اتحاد وافضل كفاءة حصاد ضوئي.

يوضح حساب الأمثلية الهندسية أن جميع أطوال اواصر أنابيب الكاربون النانوية المفردة (SWCNT) وصبغة الازو العضوية المشوبة بالنحاس متفقان مع الدراسات النظرية والتجريبية. يُظهر حساب الطاقة المدارية الجزيئية أنابيب الكاربون النانوية المفردة (SWCNT) ذات ا لأبعاد (2,2,10) و (2,2,14), استوفت شرط عملية التجديد وإعادة التركيب ، وفي الوقت نفسه ، (3,3,8) لا يمكنها توليد زوج من الكترون- فجوة يُظهر طيف UV-Vis. لهياكل SWCNT أن امتصاصية جميع التراكيب في النطاق المرئي للإشعاع الكهرومغناطيسي. تم تحسين الخواص الإلكترونية والبصرية لـ (SWCNT) (3,3,8) من خلال الاتصال بصبغة الازو المشوبة بالنحاس. نلاحظ من النتائج أن عملية التجديد وإعادة التركيب قد تم تعزيزها عندما تم توصيل (SWCNT) بصبغة الازو المشوبة بالنحاس. تم تحويل اعظم طول موجي للامتصاص من النطاق المرئي إلى نطاق الأشعة تحت الحمراء للإشعاع الكهرومغناطيسي. النتيجة النهائية يمكن استخدام تراكيب الأنابيب النانوية وصبغة الازو المشوبة بالنحاس في مجال الطاقة الشمسية.

Summary

The possibility of nanostructures of azo dye doped with (Silicon Si, Titanium Ti, Sulfur S, Zinc Zn, Aluminum Al, Copper Cu, Nickel Ni) atoms as a sensitizer of dye sensitizer solar cells DSSCs is investigated. The density functional theory with B3LYP/6-31G is used to get the geometrical optimizations and electronic properties of nanostructures. The feasibility of the nanostructures as the sensitizer of DSSC was studied by the lowest unoccupied molecular orbital LUMO and high occupied molecular orbital HOMO of the nanostructures with respect to the $I^{`}/I_{3}^{`}$ electrolyte, and TiO_2 electrode respectively, the charge spatial separation and the energy gap. The time-dependent DFT TD-DFT is used to investigate the optical absorptions and light-harvesting efficiency of the optimized nanostructures.

The results showed that all the nanostructures except azo-Al have HOMO and LUMO that satisfy the conditions of sensitizers. However, only three of the eight considered nanostructures exhibit charge spatial separation. The most azo-doped nanostructures improved absorptions in the visible region. The azo doped with the sulfur atom azo-S is recognized as the most promising applicant sensitizer of DSSCs which is most suitable LUMO and HOMO. It is characterized by charge spatial separation, low recombination rate, and good light-harvesting efficiency.

Geometrical calculation shows that all the bonds length of single-walled carbon nanotube SWCNT and Cu-doped azo organic dye agreed with theoretical and experimental studies. Molecular orbital energy calculation shows that the SWCNT (2, 2, 10) and (2, 2, 14) satisfied the condition of regeneration and recombination process, meanwhile, (3, 3, 8) can't generate pair of electron-hole. The UV-Vis. spectrum for SWCNT

structures shows that all samples were absorbed in the visible range of electromagnetic radiation. Electronic and optical properties for (3, 3, 8) SWCNT were enhanced by connecting with Cu-doped azo dye. Results conclude that the regeneration and recombination process was enhanced when SWCNT connected with Cu-doped azo dye. The maximum wavelength of absorption was shifted from the visible range to the infrared range of electromagnetic radiation. The final result express that can be used nanotube structures and Cu-doped azo dye in the solar energy field.

List of Contents

List of Figures

List of Tables

List of Symbols and Abbreviations

Symbol	Description
E	**The total energy**
KE	**The kinetic energy**
PE	**The potential energy**
M	**The mass of particle**
V	**The particle's velocity**
P	**The particle's momentum**
Ze	**The field of a nucleus of charge**
R	**The distance of the electron from the nucleus**
e	**The electronic charge**
$\hbar$	**The Plank constant (h) divided by** 2π
∇^2	**The Laplacian operator (kinetic energy operator)**
$\hat{\mathbf{H}}$	**The Hamiltonian operator**
$\mathbf{T_N}$	**The kinetic energy operators for the nuclei**
$\mathbf{T_e}$	**The kinetic energy operators for the electrons**
$\mathbf{V_{ee}}$	**The potential energy between electron-electron**
$\mathbf{V_{En}}$	**The potential energy between electron-nucleus**
$\mathbf{V_{NN}}$	**The potential energy between nucleus-nucleus**
Ψ	**The wave function**
$\mathbf{T_S[n]}$	**The Kinetic energy of a non-interacting electron**

ε_i	**The Kohn–Sham orbital energies**
$\Psi_i(r)$	**The Kohn–Sham orbitals**
$V_{xc}(r)$	**The exchange-correlation potential**
H^{core}	**The one-electron Hamiltonian**
J_j	**The direct Coulomb repulsion**
E_n	**The total energies of the ground state**
E_{cation}	**The total energies of the cation**
$E_{xc}[n]$	**The DFT exchange-correlation energy**
E_{anion}	**The total energies of the anion**
E_X^{B88}	**The Becke's exchange functional**
E_C^{LYP}	**Yang and Parr's correlation functional as gradient corrections**
STO	**Slater type orbitals**
GTO	**Gaussian-type orbitals GTO**
HF	**Hartree-Fock**
IP	**Ionization Potential**
MWCNTS	**Multi Walled Carbon Nanotubes**
SWCNTs	**Single Walled Carbon Nanotubes**
UV	**Ultraviolet**
UV-Vis	**Ultraviolet-Visible**
θ	**The bond angle between lines (j-i) and (j) at (j) (j-k)**

Chapter One

General Introudaction

1-1 Introduction

Energy is most important in today's world, as a lack of it poses a major challenge to current development (i.e. insufficient food, warm shelter, and internet access, as well as the consumption of nanotechnology products) [1]. For the design and operation of efficient systems for the generation, storage, transformation, and transportation of energy in diverse forms, promising new technologies, as well as novel physical and chemical processes, are required to extend present energy trends [2].

A number of organic and inorganic semiconductors have been used in solar cells. Because experimental data was the primary source for screening solar cell materials until recently, the selection was mostly based on known materials [3]. A lot of factors impact solar cell efficiency, including the quantity of concentrated sunlight and the stacking of multi-junction cells. The Massachusetts Institute of Technology (MIT) has created a new system that uses sunlight to heat an absorber-emitter arrangement over photovoltaic cells (PV) [4]. The worldwide mean the temperature on the ground has risen by 0.3-0.6 ^{0}C. Since the late 1800s, the worldwide sea level has increased by 10-25 cm, almost entirely due to human activity [5]. Climate change has already increased the number and intensity of regular disasters, and in the future decades, it is predicted to have considerably more severe consequences for people and other life forms all across the planet [6]. Solar cells are devices that convert solar energy directly to electricity, either through the photovoltaic effect or indirectly by first converting solar energy to heat or chemical energy [7]. Solar panels are made up of cells that are used to create solar modules, which are used to store energy from the sun. The

energy generated by these solar modules is known as solar power [8]. When the light source isn't inevitably sunlight, cells are referred to be photovoltaic cells (for example, lamplight) [9]. Second-generation solar cells use thin sheets of materials including formless silicon, cadmium telluride, and copper indium (gallium) dieselin [10]. Low-cost solar cells have been a major topic in science for the past three decades [11]. One of the most promising materials for low-cost energy generation has been discovered: amorphous semiconductors [12]. DSSCs (dye-sensitized solar cells) are a new form of low-cost energy conversion technology that uses a dye to sensitize the solar cell [13].

1-2 Elements used in the present study

Silicon Si is the chemical element with the symbol Si and atomic number 14. It is a hard, brittle crystalline solid with a blue-grey metallic luster, and is a tetravalent metalloid and semiconductor. It is a member of group 14 in the periodic table: carbon is above it, and germanium, tin, lead, and flerovium are below it. It is relatively unreactive [17]. Silicon Si was used in the initial generation of solar cell research due to its availability and applicability in the growing semiconductor sector [11]. Extrinsic n-type and p-type semiconductors are produced when intrinsic semiconductors, such as Si, are doped with one of two donors or acceptor impurity atoms [14]. By altering the atomic density of impurity atoms, the concentration of the carrier (electron or hole) and, as a result, the material conductivity can be changed [15].

Zinc Zn is a bluish-white, lustrous, diamagnetic metal though most common commercial grades of the metal have a dull finish. It is somewhat less dense than iron and has a hexagonal crystal structure, with a distorted form of hexagonal close packing, in which each atom has six

nearest neighbors (at 265.9 pm) in its own plane and six others at a greater distance of 290.6 pm. The metal is hard and brittle at most temperatures but becomes malleable between 100 and 150 °C [16].

Aluminum Al is a chemical element with the symbol Al and atomic number 13. Aluminum has a density lower than those of other common metals, at approximately one third that of steel. It has a great affinity towards oxygen, and forms a protective layer of oxide on the surface when exposed to air. Aluminum visually resembles silver, both in its color and in its great ability to reflect light. It is soft, non-magnetic and ductile. It has one stable isotope, Al; this isotope is very common, making aluminum the twelfth most common element in the Universe. The radioactivity of Al is used in radio dating [18].

Sulfur S is a chemical element with the symbol S and atomic number 16. It is abundant, multivalent and nonmetallic. Under normal conditions, sulfur atoms form cyclic octatomic molecules with a chemical formula S8. Elemental sulfur is a bright yellow, crystalline solid at room temperature [19]. Copper Cu plays an important role in these renewable energy systems. Copper usage averages up to five times more in renewable energy systems than in traditional power generation, such as fossil fuel and nuclear power plants since copper is an excellent thermal and electrical conductor among engineering metals (second only to silver), electrical systems that utilize copper generate and transmit energy with high efficiency and with minimum environmental impacts [20].

Titanium Ti is a chemical element with the symbol Ti and atomic number 22. It found in nature only as an oxide, it can be reduced to produce a lustrous transition metal with a silver color, low density, and high strength, resistant to corrosion in sea water, and chlorine [21].

Nickel Ni is a chemical element with symbol Ni and atomic number 28. It is a silvery-white lustrous metal with a slight golden tinge. Nickel is a

hard and ductile transition metal. Pure nickel, powdered to maximize reactive surface area, shows a significant chemical activity, but larger pieces are slow to react with air under standard conditions because an oxide layer forms on the surface and prevents further corrosion (passivation). Even so, pure native nickel is found in Earth's crust only in tiny amounts, usually in ultramafic rocks, and in the interiors of larger nickel–iron meteorites that were not exposed to oxygen when outside Earth's atmosphere [22].

Additionally, due to its unusual carbon allotrope features and peculiar shape, it has a wide range of possible uses, including those in electronic devices, energy storage, chemical decorations, and biosensors [20]. Researchers have extensively studied the thermal, electronic, electron transport, mechanical, and structural properties of carbon nanotubes in recent years [11]. Single-walled carbon nanotubes (SWCNTs) and multi-walled carbon nanotubes (MWCNTs) are two different forms of carbon nanotubes. MWCNT ranges in diameter from 5 to 100 nm, whereas SWCNT has a diameter of roughly 1 nm, as shown in Fig.(1. 1).

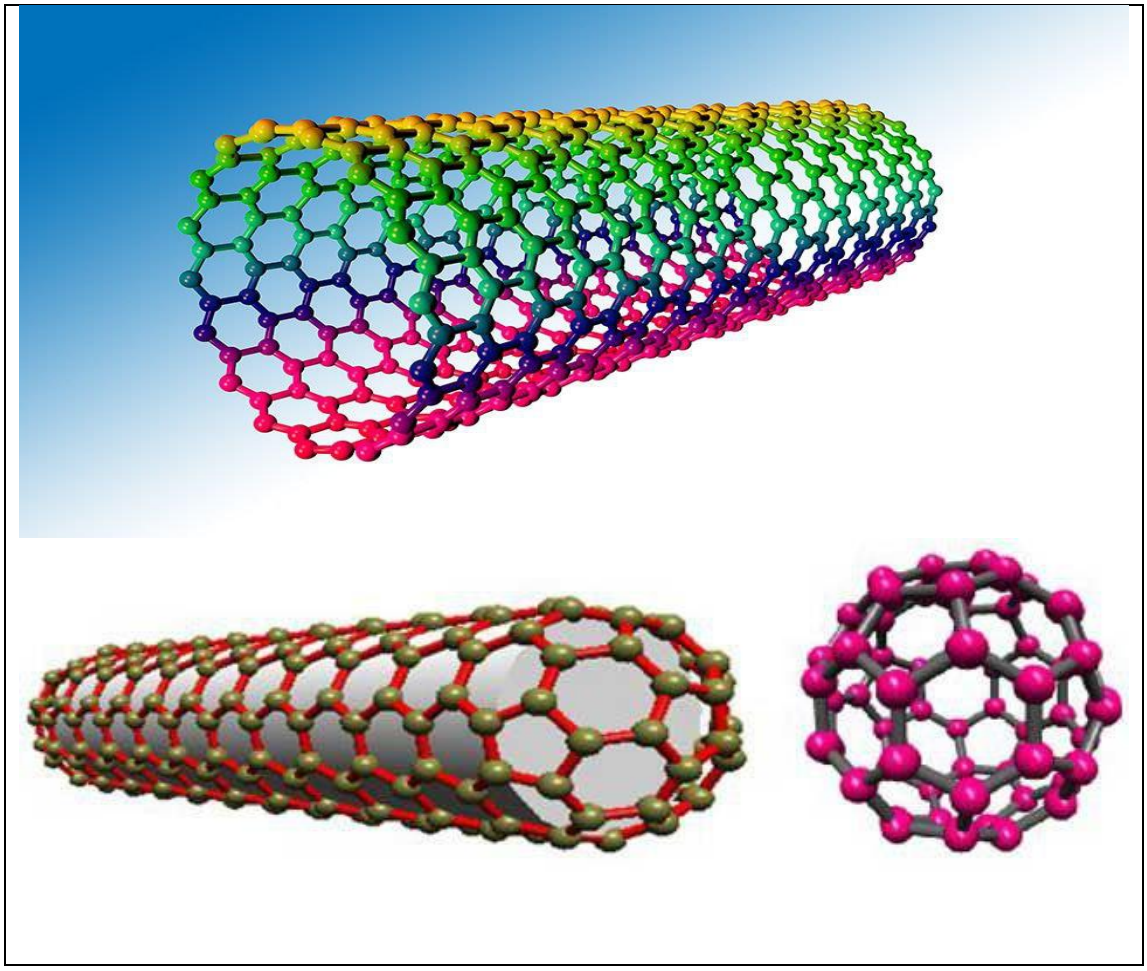

Figure (1. 1): Carbon nanotubes[12].

Heavy semiconductor doping is undesirable because it causes the band gap to narrow due to impurity sub-bands, which is detrimental. Recombination is anticipated to grow when defect states rise [23]. Since the landmark work in 1991 by O'Regan and Grätzel, the creation of energy from sun using sustainable materials like solar cells with dye sensitization (DSSCs) has attracted the interest of numerous technologies [24]. These low-cost and easy-to-make gadgets cleared the way for a new generation of economical photovoltaic modules, which have emerged as a viable alternative to silicon-based solar cells [25]. Separating light collecting and charge separating, as plants do in natural photosynthetic processes, was critical to obtaining low costs and increased functionality [26]. When opposed to the conservative fossil fuels, solar energy is one of

the most exciting and promising alternative energy sources [27]. Crystal-like silicon-based solar cells dominate the photovoltaic industry, accounting for more than 90% of worldwide solar cell output [28]. One of the most important aims in solar cell production is to keep prices low while maintaining a high conversion efficiency [29]. The materials utilized and the processing procedures employed are the two key components that must be addressed for cost reduction [30].

1-3 Azo dye

Azo dyes represent the largest production volume of dye chemistry today, and their relative importance may even increase in the future[11]. These dyes are synthesized from a simple method of diazotization and coupling. Different routes and modifications are made to obtain the desired color properties, yield and particle size of the dye for improved dispersibility. Azo dyes are the most used dyes and account for more than 60 % of total dyes approximately 70 % of all the dyes used in industry are azo dyes. Azo dyes are the most important synthetic colorants which have been widely used in textile, printing, paper manufacturing, etc. The term azo dye refers to a large class of industrial organic dyes that contain nitrogen in the form of an azo group -N = N - within their molecular structures, within the general formula R − N = N − R′, where R and R' is usually an aryl group such as Congo Red dye[10]. These pigments have different colors but are generally not very stable. These dyes are used in dyeing fabrics, leather, paper, rubber, and in the manufacture of paints, printing, etc. They are also used as evidence in analytical chemistry, and they are insoluble in water and other solvents. Azo sticks have bright colors, especially red, orange, and yellow[13]. Some azo compounds, for example, use methyl orange as a guide for acid-base reactions. Most DVD-R/+R discs and some CD-R discs use azo blue as the recording layer. Depending on other chemical characteristics, these dyes fall into

several categories based on their texture or the ways in which they are applied. The oldest method of applying azo dyes to cotton involves successive treatment with a solution of two chemicals that react together to form the dye within or on the surface of the fibers[11]. Dyes applied in this way are called show dyes. The most easy-to-apply azo dyes are those classified as direct: they contain chemical substituents that make them soluble in water and thus absorbed from the solution with cotton. The first direct dye was Congo Red, discovered in 1884, which was later largely replaced by acid and fade resistant dyes. Azo-acid dyes have an affinity for wool and silk and are applied by the same procedure used for direct layering. An example is tartrazine, a yellow-colored azo-acid dye discovered in 1884 and still in common use. Other azo dyes contain chemical groups that bind to metal ions. Of the many metal salts used with these dyes, chromium and copper are the most common; Often, the metal ion also combines with the fiber, improving the dye's resistance to washing .Azo dyes are shown in Fig. (1. 2)[13].

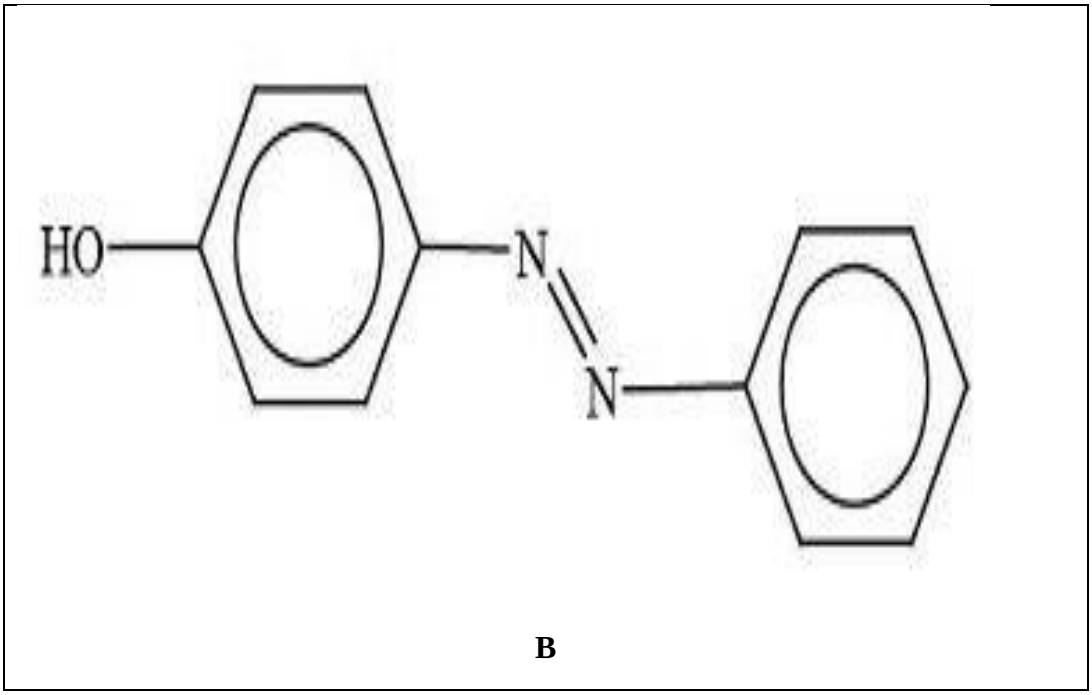

B

Figure (1. 2): Azo dye chemical structure [6].

1-4 Types of Solar cells

There are two types of solar cells inorganic and organic.

1-4-1 Inorganic Solar Cells

The percentage of crystal-like silicon cells made from p-type material is close to 95%, while the percentage of crystal-like silicon cells made from n-type material is just little more than 5% [31]. This is mostly owing to a lack of industrial application of n-type cell techniques for multi-crystalline substrates and insufficient growth [32]. However, n-type silicon materials have lately attracted a lot of attention as potential candidates for future generations of high-efficiency solar cells [33]. Despite the fact that n-type crystalline silicon solar cells are in short supply sun power and Sanyo, two prominent producers, are employing this material to make high-efficiency solar cells [34]. The efficiency of these cell types were 24 and 23 percent, respectively [35]. The reflection of light from the air/silicon contact reduces solar cell efficiency significantly. As a result of this reflection, the outer quantum efficiency is lowered [36]. An sufficient amount of antireflection coating can be utilized to match the optical impedance and reduce reflection [37]. The antireflective coating SiN_x is the most extensively used and widely available [38].

1-4-2 Organic Solar Cells

Organic solar cells has grown interest due to their ease of processing [33], because polymer processing science has progressed, traditional processing technologies like as roll-to-roll processing and doctor-blading are expected to be employed in the future to create large-area, low-cost organic solar cells on flexible substrates [39]. Flexible cells, according to the researchers, might be employed in a range of applications, such as portable electronics and commercial power generation [40], because of

their adaptable chemical composition and simplicity of manufacturing for large-area photovoltaic panels, organic solar cells are appealing possibilities for harvesting solar energy [41]. Organic semiconductors, which are commonly found in organic/polymer mixes with band gaps ranging from 1.4 eV to 3 eV and absorb a tiny portion of the solar spectrum, are the basis for these materials. Stacking cells with various band-gaps in sequence is one way to get around this restriction [23]. New materials and devices with lower band gaps, on the other hand, involve meticulous design, and understanding diffusion dynamics is required to improve solar cell efficiency. Poor stability, even after encapsulating to guard against oxidation, has impeded the creation of novel and efficient organic devices .Spin-coating, doctor blading, and screen-printing technologies were used to create organic solar cells [42]. The use of large-scale printing and coating processes allows production to be ramped up while using less energy [43]. This has implications for the amount of energy provided by a solar cell during its lifespan, conversely the amount of energy required to manufacture the same solar cell is referred to as the global energy balance [39]. The quest for high-efficiency, low-cost solar photovoltaic technologies has prompted organic solar cells, dye-sensitized solar cells, quantum dot solar cells, and other technologies are undergoing extensive study and development [44]. Organic solar cells have a number of benefits over other emerging alternative organic solar cells, including low cost, plentiful earth components, easy production techniques, and the ability to include a variety of other technologies [45]. Organic solar cells now have the greatest documented efficiency of over 10%, and it is commonly accepted that their lower operational efficiency compared to traditional silicon solar cells does not limit their commercialization potential due to their advantage [46]. Organic solar cells' core physics, functioning mechanism, and latest advances [47].

Solar cells are now more expensive than traditional energy sources, which is a big drawback [48]. To address budgetary restraints, researchers are working to improve solar cell efficiency as well as develop and commercialize lower-cost materials [49]. While silicon performs well in solar cell applications, it takes a lot of energy to turn it into crystalline wafers, because silicon wafers are so expensive [50]. Many researchers are looking for other materials to serve as the basic semiconductors in solar cells[51]. Nanoscale science's present success has supplied researchers with novel fabrication techniques, materials, and probing tools, allowing for unprecedented control over the structure and dynamics of solar cells to convert solar radiation into electrical energy, a DSSC drives through three steps as shown in the figure(1.3), it is based on photo-excitation of dyes activating an electron transfer into the conduction band of semiconductor such as TiO_2, followed by regeneration of oxidized dye molecules via electron donation from the redox couple in the electrolyte, and lastly migration of electrons through the exterior load [52].

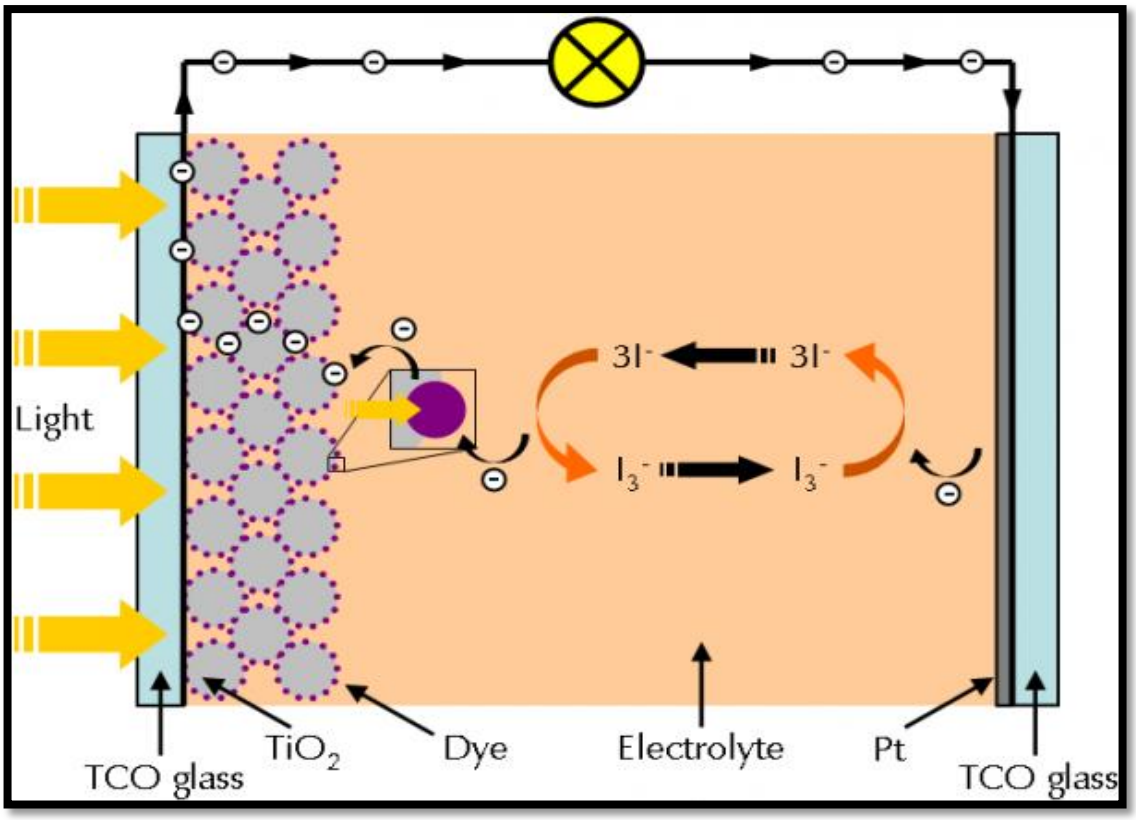

Figure (1. 3): Fundamental process of dye sensitizer solar cells (DSSCs)[8].

1-5 Previous studies.

- **Regimol C. Chen and et al. [53], in(2007)** used Phtlialocyaiunes to make organic dye lasers. The examination of the optical characteristics of these thin films is required for application in thin films optics. Tin phllialocyanine (SiPc) thin films produced by thermal evaporation were utilized in the characterization investigations. The absorption spectra are utilized to look into how heat radiation and post-deposition heat treatment affect the optical band gap.
- **S. Cataldo and et al. [54], in (2012)** investigated many challenges relating to their synthesis, purification, functionalization, processing, and device integration, using carbon nanotubes in photovoltaics is still a challenge, review chosen contributions dealing with the aforesaid

difficulties initially, then concentrate on the benefits and limitations of carbon nanotubes in the creation of organic solar cells.

- **Wei-Lu Ding and et al. [55] , in (2013)** studied the optical efficiency of the indoline dye by density function theory and time depending-self consist field. Six types of indoline dye doped with π-spacer. The researchers investigated solar energy conservation efficiency, open voltaic circuit, light harvesting, injection free energy, redox potential and wavelength of absorption. Result showed that all indoline dye structure are satisfy regeneration and recombination process because of all LUMO level distribute above CBM(TiO_2) and HOMO below I/I_3. All molecular structure absorbed in the visible region of electromagnetic radiation. Meanwhile, indoline dyes molecular structure have high values of open voltaic circuits varies from (0.82 - 1.82) Volt.
- **S. Zhang and et al. [56]**, **in (2013)** High energy conversion efficiency is one of the most important keys to the commercialization of dye-sensitized solar cells (DSCs) in the huge electricity generation market. According to our experience in the persistent efforts that helped to achieve high efficiency DSCs, selectively review the major progress of improving the energy conversion efficiency of DSCs which may be useful for future applications. We start the discussion from modeling the device by macroscopic equivalent circuit and then highlight some approaches to improve the device performance, such as the molecular engineering of novel dye sensitizers and light trapping effect, tuning the potential of redox shuttles and surface passivation of photoelectrodes, and optimizing the resistance. illustrate a roadmap of possible future directions of DSCs with the challenges of how to further improve the efficiency to accelerate the progress in the commercialization of DSCs.

- **S . Shalini et al.** [**57**] **, in (2016**) discovered as sensitizers, DSSC currently employs inorganic Ruthenium (Ru)-based, metal-free, and natural dyes. Due to their inexpensive cost, simplicity of preparation, accessibility, and environmental friendliness, metal-free and natural dyes have become a potential alternative to expensive and scarce Ru-based dyes, because of their narrow absorption bands (100-250) nm, undesired dye aggregation, and instability, most alternatives to Ru-based dyes have so far shown to be inferior to Ru-based dyes.
- **J. Day et al.** [**58**]**, in (2018)** investigated the spectral mismatch between solar cells and incident radiation is a crucial element that limits their efficiency, according to research. Materials and luminescent processes exist that can alter the characteristics of incident sunlight to better suit the cell's best absorption zones. This is a fascinating field of research and a promising strategy for improving solar cell efficiency, which is critical for environmental reasons organic solar cells.
- **F. Gao et al. [59], in(2018)** studied the geometrical, electronic and optical properties for graphene-dye organic composites by density function theory method. Structural properties show that all bond lengths were being an agreement with experimental measurements. Electronic properties show that all HOMO energy level was distribution below iodine/tri-iodine redox potential and LUMO was distributed above minimum conduction band of titanium dioxide. Result indications all system was had an ability to generate electron-hole process. Time depending-density function theory calculation show that all proposed system absorbed in visible region of electromagnetic radiation. Meanwhile, result prove that all proposed system were more suitable for application in dye sensitized solar cells field.
- **L. Michels et al. [60], in (2021)** studied the crystal structure and optical properties for curcumin, bixin and indigo dyes and applicable in

solar energy field. X-Ray diffraction calculation show that curcumin dye has wide degree of crystallization compared with bixin and indigo dyes. Evaporation calculation shows that bixin was distraction chemically and indigo and curcumin dyes doesn't appear any change in structure. The calculation of photo emission ultra violet spectra show that indigo dye has negative work function and ionization potential. Result shows that it can ability design photo detectors from three dyes used in the study.

- **A. Behera and et al.** [**61**]**, in (2022)** used quantum chemical simulations to investigate the impact of heterocyclic spacers on azo-based metal-free donor-acceptor dyes. To create twelve distinct dye sensitizers, six heterocyclic moieties were added to an azo-based dye in two different places as extra spacers. The advancement on the optoelectronic characteristics and the effectiveness of such dyes have been explored using a density functional method,computed characteristics, including those related to charge transfer analysis, light-harvesting efficiency, and driving.
- **K. Periyasamy and et al. [62], in (2022)** studied the optical efficiency conservation of the phenothiazine and dibenzofuran dyes by the time depending-density function theory calculations. The electronic properties show that two dyes under study have high ability to inject the electrons to electrodes also, molecular orbitals energy satisfy the conditions of regeneration and recombination phenomena and absorbed in the visible range of electromagnetic radiation.

1-6 Aims of the present study

The aims of the present study can be summarized by two points

1- Constructing the nanostructures of azo dye and azo doped with (Si, Ti, S, Zn, Al, Cu, Ni) atoms as DSSC by using DFT with B3LYP/6-31G, and investigating the photosensitizer performance of these nanostructures.
2- Examination the photosensitizer performance of single walled carbon nanotubes SWCNTs and SWCNT/ Cu- azo dye.

Chapter Two

Theoretical Background

2-1 Introduction

Theoretical calculations in physics and chemistry are commonly employed when a mathematical method has been sufficiently developed and may be applied using a computer [63]. The fundamental laws of physics are linked with mathematical approaches in theoretical chemistry to analyze chemical progressions. Computational physics and chemistry, often known as molecular modeling, is a discipline of chemistry in which computers are used to mimic molecules [64]. It is an important and basic element of molecular science research. Molecular modeling methods and physicians are now widely used to investigate computationally many properties such as molecule energies, molecular geometries, electronic structure, electron and charge distributions, Infrared (IR), Ultraviolet (UV), and physical properties of biological, inorganic, organometallic, polymeric, catalysis drug, and other molecular systems [65]. The four primary approaches used by computational chemists and physicians are density functional theory (DFT)[66]. Density functional approaches are at the heart of today's atomic, molecular, solid-state, and even nuclear physics computation as a result of their widespread success, these methods are used by a huge number of computational physicists [67]. Density functional conceptions dominated mathematical physics in the 1970s (Thomas-Fermi theory), 1980s (Hohenberg-Kohn theory), and 1990s (density functional theory). Computational chemistry involves the study of molecular geometries, molecule energies, chemical reactivity, IR spectrum, UV spectrum,, as well as the physical characteristics of substances [68].

2-2 Schrödinger equation

Schrödinger's immediate focus when developing his equation to treatment the hydrogen atom, and the solution reached in 1926 convinced him. The creation of a wave equation that may describe stealthy, wave-like behavior of the first step is to create a quantum particle. In developing a theoretically consistent theory of nonrelativistic quantum mechanics. The Schrödinger equation is the name for this equation [69]. In quantum physics, the Schrödinger equation has a similar role to in classical mechanics. Schrödinger equation is a partial differential equation that describes how a quantum particle's wave function ebbs and flows. Newton's second law is a differential equation that outlines how a classical particle moves [70]. In addition, both Newton 's laws and Schrödinger equation were suggested and then evaluated for time-independent systems, where total energy(E) is equal to the sum of total kinetic and potential energy[68]:

E = KE (kinetic energy) + PE (potential energy) (2.1)

The kinetic energy of an electron is calculated as follows[69]:

$KE=(1/2)mv^2=p^2/2m$ (2.2)

Where m denotes particle mass, v denotes particle velocity, and p denotes particle momentum. The electron travelling in the charge's field Ze nucleus has a potential energy of [70]:

$PE = -Z\ e^2\ r^{-1}$ (2.3)

Where r is denotes to the electron's distance from the nucleus and e denotes the unit of electronic charge. As a result, the electron's total energy is [70]:

$$E = \frac{p^2}{2m} - Ze^2 r^{-1} \quad (2.4)$$

a kinetic energy contribution and a potential energy function added together [68]:

$$\left\{-\frac{\hbar^2}{2m}\nabla^2-\frac{Ze^2}{r}\right\}\psi(r)=E\psi(r) \tag{2.5}$$

Where:

$\hbar$: Plank constant (h) divided by 2π.

Ψ : The wave function of an electron.

∇^2 :The Laplacian operator is a kind of operator (kinetic energy operator).

Eq. (2.5) denotes the Hamiltonian operator, denoted by the letter $\hat{H}$. Schrödinger equation is written in condensed form as [71]:

$$\hat{H}\psi(r)=E\psi(r) \tag{2.6}$$

A Hamiltonian operator with a large number of electron atoms can be expressed in a similar way. It's the total of the nuclei and electrons kinetic energy operators, as well as the potential energy terms indicating the numerous Columbic interactions [72]:

$$H^T = T_N + T_e + V_{ee} + V_{eN} + V_{NN} \tag{2.7}$$

Where the kinetic energy operators for nuclei and electrons are T_N and T_e, respectively. The potential energies of electron-electron, electron-nucleus, and nucleus-nucleus, respectively, are V_{ee} , V_{eN} and V_{NN}.

Suppose that there are N nuclei with n electrons, the total Hamiltonian operator will be in atomic units [70]:

$$H^T=-\frac{1}{2}\sum_A^N\frac{1}{M_A}\nabla_A^2-\frac{1}{2}\sum_p^{2n}\nabla_p^2+\sum_{p<d}^{2n}r_{pd}^{-1}-\sum_A^N\sum_p^{2n}Z_A r_{Ap}^{-1}+\sum_{A<B}^N Z_A Z_B R_{AB}^{-1} \tag{2.8}$$

Where M_A is the mass of nucleus A; m electronic mass; Z_A, Z_B are the charges on nuclei A and B, respectively, r_{pd} is the distance between p and d electrons, and R_{AB} is the distance between nuclei A and B. The general form of Schrödinger equation will be [73]:

$$H^T(1,2,\ldots,N,1,2,..,n)\ \Psi(1,2,\ldots,N,1,2,..,n)=E\Psi(1,2,\ldots,N,1,2,..,n) \qquad (2.9)$$

Where $\Psi(1,2,\ldots,N,1,2,..,n)$ is the entire wave function for all particles in the molecule and is the overall energy of the system.

2-3 The Wave Function

The wave function Ψ is not physically observable, but its square $[\Psi]^2$ can be interpreted as the probability density, which yields a probability when multiplied by the volume of a region. Acceptable wave functions for a system have to:

1. Orthogonal one to another.

2. Normalized.

3. Form a complete set.

"Orthonormality" refers to the characteristic that wave functions have: $\int \Psi_i^* \Psi_j dx_N = \langle \Psi_i | \Psi_j \rangle = \delta_{ij} \equiv \begin{cases} 1, if\ i = j \\ 0, if\ i \neq j \end{cases}$ (2-10)

Completeness refers to the ability to create the "delta function," which is the sharpest possible function of the unit area, from the whole set of eigen functions. The energy of a wave function can be calculated using the Hamiltonian operator's predicted value [74,75].

$$E = < \hat{H} > = \frac{\int \Psi^* \hat{H} \Psi \, dv}{\int \Psi^* \Psi \, dv} \qquad (2\text{-}11)$$

The wave function Ψ describes the many-particle systems.

2-4 Hartree - Fock (HF) Approximation

Pauli exclusion principle should be considered when applying Schrödinger equation with an atoms multiple electrons, molecules or solids. The sign of the wave function must be flipped when the coordinates of any two electrons are changed, according to this concept. The wave function becomes antisymmetric as a result of this. Hartree was the first to derive the many-electron Schrodinger equations. The whole wave function, according to Hartree, could be approximated as a sequence of one electron wave functions [76].

$$\Psi_{tot} = \prod_{i=1}^{n} \Psi_i (x) \tag{2.12}$$

Pauli exclusion principle was not taken into account in Hartree equations. Fock and Slater updated this method to include the influence of electron exchange and the exclusion principle; as a result, using the Slater determinant, the entire wave function for n electron systems is produced in the form [77]:

$$\Psi(1,2,\dots,\mathrm{n}) = \frac{1}{\sqrt{\mathrm{n!}}} \begin{vmatrix} \Psi_1(x_1) & \Psi_2(x_1) & \dots & \Psi_\mathrm{n}(x_1) \\ \Psi_1(x_2) & \Psi_2(x_2) & \cdots & \Psi_\mathrm{n}(x_2) \\ \vdots & \vdots & \ddots & \vdots \\ \Psi_1(x_n) & \Psi_2(x_n) & \cdots & \Psi_\mathrm{n}(x_n) \end{vmatrix} \tag{2.13}$$

Hartree-Fock equations, often known as self-consistent field equations, are a type of self-consistent field equation. These equations are formatted as follows:

$$[H^{core} + \sum_j \left(2J_j - K_j\right)]\Psi_i = \sum_j \varepsilon_{ij}\Psi_j \qquad \mathrm{i} = 1,\dots,\mathrm{n} \tag{2.14}$$

The left-hand side of Eq. (2.14) is also known as the Fock Hamiltonian since it reduces Eq. (2.14) to the standard form.

$$F\Psi = \sum_j \varepsilon_{ij}\Psi_j \qquad \mathrm{i} = 1,\dots,\mathrm{n} \tag{2.15}$$

Trial wave functions are utilized to construct the Coulomb and exchange potential integrals and differential equations in order to solve the n Hartree-Fock equations. Solving the n equations yields a new set of wave functions. After that, the new wave functions are utilized to compute a new set of potential integrals. The cyclic approach is repeated until the estimated wave functions or potential integrals remain unchanged. Because the final wave functions yield potential integrals, which, in turn, produce the identical wave functions within a specified acceptance, When Eqs. (2.15) are solved, this approach is known as the self-consistent field method [78,79].

2-5 Density functional theory

Quantum mechanical method of density functional theory (DFT) is frequently used to study the electronic structure of many-electron systems in physics and chemistry. It is presently one of the most important techniques for determining the ground-state properties of metals, semiconductors, and insulators [80]. DFT is one of the most extensively used and useful computational methods in physics and chemistry. Thomas-Fermi model provided the foundation for the theory of density; in 1927, Thomas and Fermi described an atom's energy as a function of electron density, combining this with the standard equations Nuclear-electron interactions and electron-electron interactions may both be expressed in terms of electron density [81]. DFT concentrates on the much less complicated electron density (r). For a particular state, the number of electrons n per unit volume is the definition of electron density,the system is solely affected by three coordinates, regardless of the amount of electrons in it [80]:

$$N = \int \rho(\vec{r}) d\vec{r} \qquad (2.16)$$

Ground state energy is at the heart of DFT, and the density of electrons dictates all other ground state electronic characteristics. The electronic density corresponds with the system's exact ground conditions when the total energy is low [82, 83].

2-6 Kohn-Sham Equations

Theorems of Hohenberg and Kohn (HK) allow FHK to be written in a variety of ways [81]:

$$F[n]=T_S[n]+J[n]+E_{NC}[n] \qquad (2.17)$$

Where T_S [n] is the Kinetic energy of a non-interacting electron system. A single Slater determinant of orbitals represents the electron density of the non-interacting system. The exchange-correlation (non-classical) energy E_{xc}[n] of interacting electron system can be defined in the form[82]:

$$E_{xc}[n]=T[n]-T_S[n]+E_{NC}[n] \qquad (2.18)$$

Where E_{xc} [n]: the DFT exchange-correlation energy. By applying the variation principle, $\partial E/\partial n(r) = 0$, to the Kohn–Sham functional [83]:

$$E[n]=\int n\, V_{(r)}dr+T_S[n]+J[n]+E_{xc}[n] \qquad (2.19)$$

The density n(r) is given by [80]:

$$n(r)=\sum_{i=1}^{n}|\Psi_i(r)|^2 \qquad (2.20)$$

This leads to the Hartree-type of one–electron equations [83]:

$$[-\frac{1}{2}\nabla^2+V(r)+\int\frac{n(r)}{|r-\bar{r}|}d\bar{r}+V_{xc}(r)]\Psi_i(r)=\varepsilon_i\Psi_i(r) \qquad (2.21)$$

Where ε_i Kohn–Sham orbital energies, $\Psi_i(r)$ is Kohn–Sham orbitals, and V_{xc} (r) is the exchange-correlation potential [84]:

$$V_{xc}(r) = \frac{\delta E_{xc}[n]}{\delta n} \tag{2.22}$$

The Eqs. (2.20)–(2.22) are Kohn-Sham equations, are technically precise and only have one unknown term, E_{xc} [n] [85].

The basic goal of DFT is to discover the exchange-correlation energy E_{XC}, which has only been utilized as a mathematical word thus far. If the precise exchange-correlation function is known, the system can be solved appropriately. As previously stated, this function is generated from the difference in Hamiltonians between interacting many-electron systems and non-interacting single electron systems. As a result, this phrase encompasses all consequences of exchange and correlation interactions, such as Pauli exclusion between electrons with the same spin orientation and the instantaneous response of electrons with opposite spins [86]. Kohn–Sham equations are said to have a circular aspect to them. To solve Kohn–Sham equations, Hartree potential must be determined, and the electron density must be known to define Hartree potential. However, single-electron wave functions must be differentiated in order to calculate the electronic density, and the Kohn–Sham equations must be solved to determine these wave functions [87].

2-7 B3LYP Functional

This is the most popular DFT model. This method is called to be a hybrid, because it uses corrections for both gradient and exchange correlations. The most popular hybrid functional, B3LYP [88] uses Becke's exchange functional (E_X^{B88})1988 and Lee, Yang and Parr's correlation functional

(E_C^{LYP}) as gradient corrections to the LSDA exchange and correlation functionals [89]:

$$E_{XC}^{B3LYP} = (1-a)E_X^{LSDA} + aE_{XC}^{HF} + bE_X^{B88} + cE_C^{LYP} + (1-c)E_C^{LSDA} \quad (2.23)$$

Where the three parameters, a =0.20, b=0.72 and c=0.81.

The first parameter (a) specified the amount of exact exchange, while (b) and (c) control the contribution of exchange and correlation.

2-8 Basis sets

A basis set consists of a collection of functions used to explain the orbital structure of an atom. Linear combinations of base functions and angular functions are used to build molecule orbitals and full wave functions. Most semi-empirical techniques rely on a set of predefined bases. A collection of bases must be described after ab initio or density functional theory computations. Although a set of basis can be developed from scratch, the vast majority of calculations are performed with pre-existing basis sets. The type of computation used and the basis selected are the two most important aspects in determining the correctness of the results [85]. Slater type orbitals(STO) are exponential that mimic the exact eigen functions of the hydrogen atom. A typical STO is expressed as [53,76]:

$$\chi^{STO} = Nr^{n-1}e^{-\xi r}Y_{lm}(\theta,\varphi) \quad (2.24)$$

(STOs) satisfies all the appropriate boundary conditions, having a cusp at the nucleus and exponentially decaying to zero at infinity.

Gaussian-type orbitals (GTOs) can be written in terms of Cartesian coordinates as [76]:

$$\chi^{GTO} = Nx^{l_x}y^{l_y}z^{l_z}e^{-\xi r^2} \quad (2.25)$$

2.8.1 Minimal *Basis Sets*

The minimal basis set is the minimum number of basis functions χ needed to describe the ground states of the atoms in a molecule. Common minimal basis sets are STO-NG, where N=(2-6) is the number of Gaussian primitive functions that comprise a single basis function,for example, STO-2G, STO-3G, STO-6G [53,75,80]. In these basis sets, the same number of Gaussian primitives comprises core and valence orbitals. Minimal basis sets typically give rough results that are insufficient for research quality publication but are much cheaper than their larger counter parts.

2-8-2 Split-Valence Basis Sets

In this type, the inner-shell atomic orbitals are represented by one basis function, and the valence orbitals are represented by two or more basis functions [53,75,81,82]. Split-valence basis sets employ more than one basis function of variable orbital exponents for each valence orbital and only one basis function for each core orbital. For instance, the valence double-zeta (VDZ) basis set uses two functions per valence orbital, while the valence triple-zeta (VTZ) uses three, and so on. For example, the 4-31G basis set uses a set of four primitives contracted to one basis function for each core orbital and a split-valence of three and one primitive for the valence orbitals. Another example of these are the 6-311G basis set uses a set of six primitives contracted to one basis function for each core orbital and a split-valence of three, one and one primitive for the orbitals.

2-9 Electronic properties

In this section the electronic properties will be presented.

2-9-1 Geometrical structures

All molecules possess geometry, characterized by:

1. The number and kinds of atoms.

2. Bonds' number and types.

3. Bond lengths that are relevant r : $0 \leq r \leq \infty$.

4. Bond aspect that is relevant θ: -180º $\leq \theta \leq$ 180º (units of degrees).

Geometry optimization is a physical chemistry computation that determines the lowest energy or most relaxed conformation of a molecule. The approach is an iterative process in which the molecular shape is changed slightly at each stage and the energy of the molecule is compared to the preceding cycle. The computer gently pushes the molecule in order to achieve the most relaxed condition possible. Calculates the energy, then pushes it a bit further till the lowest energy is determined. At the ideal geometry, the molecule's energy minimum is discovered [85].

2-9-2 HOMO, LUMO and energy gap

The highest occupied molecular orbital (HOMO) and the lowest unoccupied molecular orbital (LUMO) are the two most important molecular orbitals .

The band gap is the difference of the energies between the two orbitals HOMO and LUMO [90].

$$E_{gap} = E_{LUMO} - E_{HOMO} \qquad (2.26)$$

The energy gap is used to characterize the chemical reactivity and stability of a molecule, as well as to control how it interacts with other species. A tiny band gap molecule is usually associated with high chemical reactivity, low stability, and a soft molecule [91].

2-9-3 Total energy, Electron affinity, and Ionization Potential

The sum of all total kinetic and potential energy in a system is called total energy. Because the resultant of the effective forces is zero, an optimized

molecular system must have the lowest total energy value. This indicates that the molecular system is at equilibrium. The amount of energy produced when an electron attaches to an atom or moleculeXg and forms a negative ion is known as the electron affinity EA[30]:

$$X(g) + e^{-} \rightarrow X^{-}(g) \tag{2.27}$$

The IP Ionization Potential and EA can be calculated as[92]:

$$IP = E_{cation} - E_{n} \tag{2.28}$$

$$EA = E_{n} - E_{anion} \tag{2.29}$$

Where E_{n} , E_{cation} , E_{anion} are the total energies of the ground state of a neutral molecule, cation and anion, respectively.

In this study, the IP and EA are estimated according to Koopmans' theorem as[93]:

$$IP= -E_{HOMO} \tag{2.30}$$

$$EA = -E_{LUMO} \tag{2.31}$$

Where E_{HOMO} and E_{LUMO} are the HOMO and LUMO energies, respectively [92, 93].

2-10 Infrared Spectrum

Normal oscillations accompanied by variations in dipole moments are active, and they can be seen in the infrared spectrum. To absorb and emit energy, the normal modes of the simple harmonic oscillator are used to describe the oscillation of a molecule. The infrared spectrum (IR) is electromagnetic radiation in the infrared wavenumber range.$(1-5) * 10^{3}$ cm^{-1} [32]. When enough energy is absorbed by the N-atoms system, it oscillates with three degrees of freedom for translation and rotation, and

(3N-6) degrees of freedom for ring molecule vibration. Fundamental and nonfundamental oscillation bands can be observed in a system's oscillations [94]. The vibration analysis is valid only when the first derivative of the energy with respect to the atoms' displacement is zero. The method works in transition phases and higher order saddle points as well [95].

2-11 UV- Visible radiation

The excitation of electrons in both atoms and molecules from lower to higher energy levels is connected to the absorption of visible (Vis) and ultraviolet (UV) light. Because matter's energy levels are quantized, only light with precisely the right amount of energy can drive transitions from one level to the next. Ultraviolet radiation is a type of radiation that exists just below the visible spectrum of light. It has a range of wavelengths from 100 to 400 nanometers [96]. Specific compounds absorb UV or visible rays. Different molecules are capable of absorbing different wavelengths of light. Within the molecule, an absorption spectrum should show a range of absorption bands that correspond to the structural groups [97].

2-12 The programs used

2-12-1 Gaussian Program

Gaussian is a quantum physics and chemistry software suite that may be purchased from Gaussian, Inc. Almost every computer platform, including Microsoft Windows, can run the software. Web-based interface tools like Web MO can also be used to access it. According to the North Carolina School Computational Chemistry website, Gaussian is the most advanced tool available to student researchers. The '09' alludes to the

software's initial release, which occurred in 2009. The version G09 is not the most recent [98].

2-12-2 Gaussian View 5.0.8 Program

The Gaussian view program is designed to ingest Gaussian program input files and show Gaussian program output files in a three-dimensional picture. It is not a calculator, but it makes working with Gaussian algorithms simpler and offers three important advantages to users.

First: It allows the user to draw molecules, including the largest, as well as rotate, transfer, and change their size using the mouse.

Second: The Gaussian view allows for and achieves various Gaussian calculations, allowing for sophisticated input preparation for ordinary tasks and advanced methods.

Third: The Gaussian view allows to inspect the results of Gaussian computations using a variety of geometrical techniques, including the following: (Molecular orbits, electronic density surfaces, and balanced molecular patterns) [99].

2-13 Solar cell sensitizer parameters

Preference of Dye Sensitizer Solar Cell (DSSC) is evaluated by Incident Photon to Conservation Energy (IPCE). It is associated with charge collection efficiency (η_e), electron injection efficiency (φ_{Inj}) and Light Harvesting Efficiency (LHE). LHE computed from following equation [40].

$$LHE=1-10^{-f} \qquad (2\text{-}32)$$

where f is oscillation strength corresponding to maximum wavelength absorbed. Electron injection efficiency φ_{Inj} is directly proportional to free energy of electron injection (ΔG_{Inj}) [15].

$$\varphi_{Inj} \alpha f(-\Delta G_{Inj}) \quad (2\text{-}33)$$

equation (2-33) shows that more positive value of ΔG_{Inj} the grater will electron injection efficiency. Free energy electron injection is defined as difference between oxidation potential energy of excited state (E^{dye*}) and reduction potential energy of TiO_2 conduction band equal (-4.0) eV which describe by[55].

$$\Delta G_{Inj=} E^{dye*} - (E_{CB})_{TiO2} \quad (2\text{-}34)$$

E^{dye*} can be calculated by the following equation.

$$E^{dye*=} E^{dye} - \Delta E_{(\lambda max)} \quad (2\text{-}35)$$

Where E^{dye} is (-HOMO) in ground state and $\Delta E_{(\lambda max)}$ is absorption energy corresponding to maximum wavelength.

V_{oc}, can be calculated based on electron injection from the LUMO level of dye to the conduction band minimum (CBM) of TiO_2 [98].

$$V_{OC}= \text{LUMO (system)} - (CBM)_{TiO2} \quad (2\text{-}36)$$

Regeneration driving force (ΔG_{reg}) can be calculated from the difference between the ground state oxidation potential and redox potential of the iodide/tri-iodide redox couple I/I_3 computed by the following equation [100]:

$$\Delta G_{reg}=I/I_3 - E^{dye} \quad (2\text{-}37)$$

Chapter Three

Results and Discussions

3-1 Introduction

DFT calculation estimate to computing ground and excitation properties for all structures by using hybrid function B3YLP at basis set 6-31G. The present study includes three parts:

- Azo dye and azo doping with (Si, Ti, S, Zn, Al, Cu, Ni) atoms.
- Different types of single walled carbon nanotubes (SWCNT).
- SWCNT and azo dye.

3-2 The work scheme

The work scheme of the present study will be summarized by the figure(3.1).

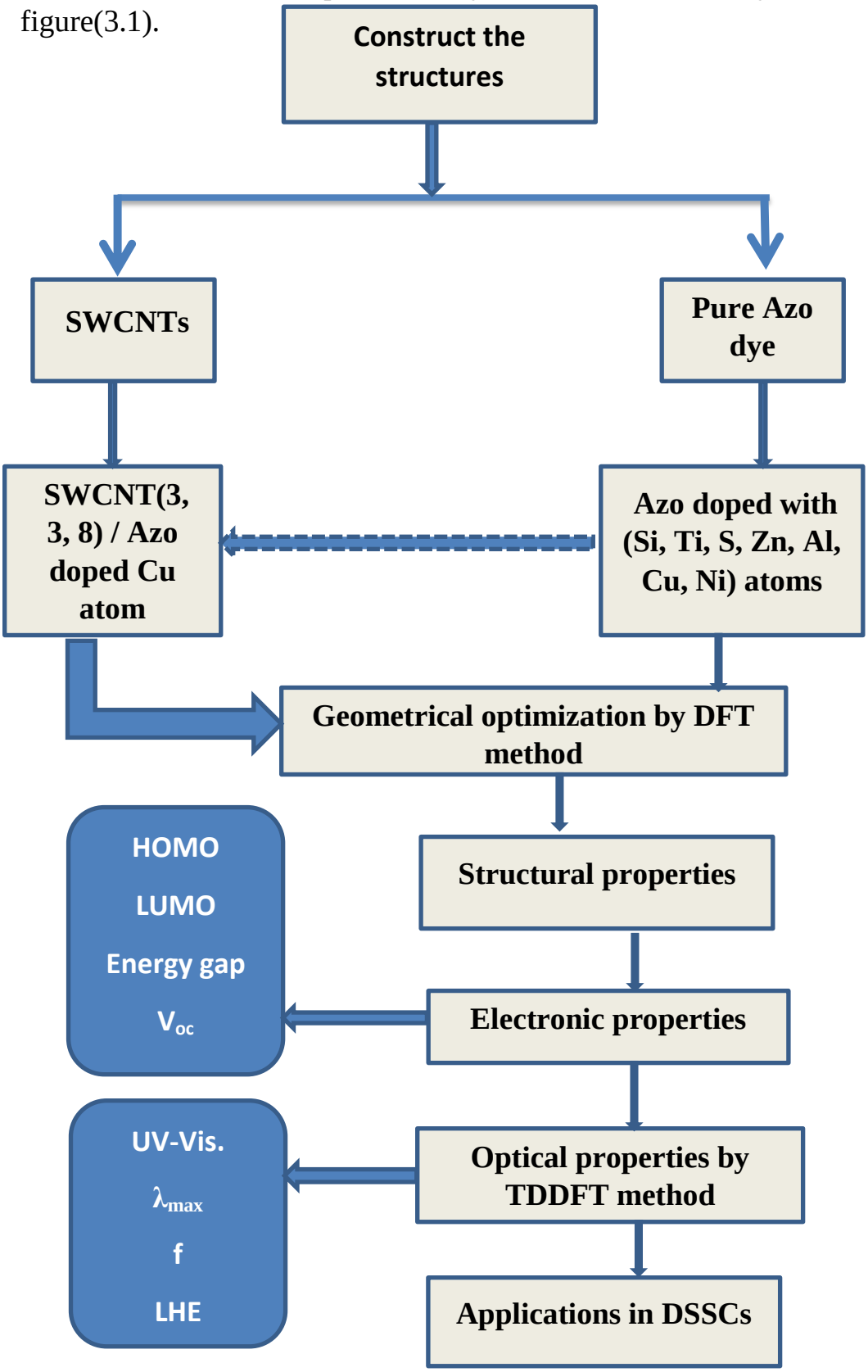

Figure(3-1): The work scheme

3-3 Computational Method for Azo Dye and Azo Doping

Nanostructures from azo dye and azo doping with (Si, Ti, S, Zn, Al, Cu, Ni) atoms are constructed. These nanostructures are completely optimized using Gaussian 09 program. The time-dependent density functional theory (TD-DFT) is used to examine the UV-Vis spectrum and calculate light-harvesting efficiency (LHE) by using the relation(2-32) [101]. The optimized nanostructures are shown in Fig.(3-2).

Pure azo

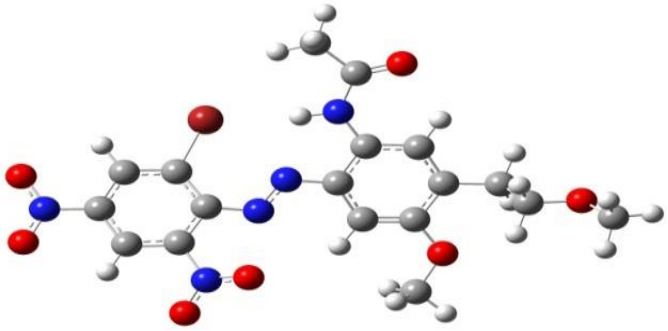

Azo-Si

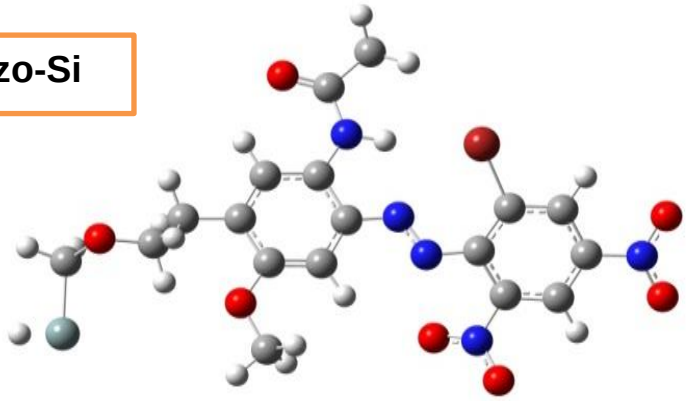

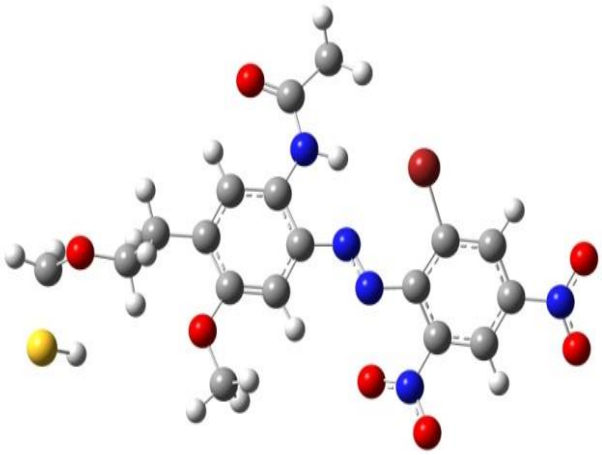

Azo-Ti

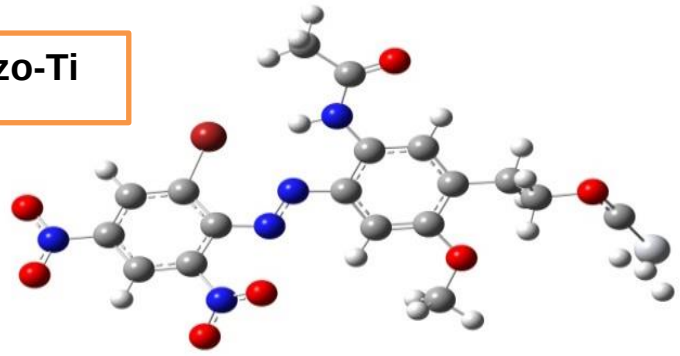

Azo-Al

Azo-Zn

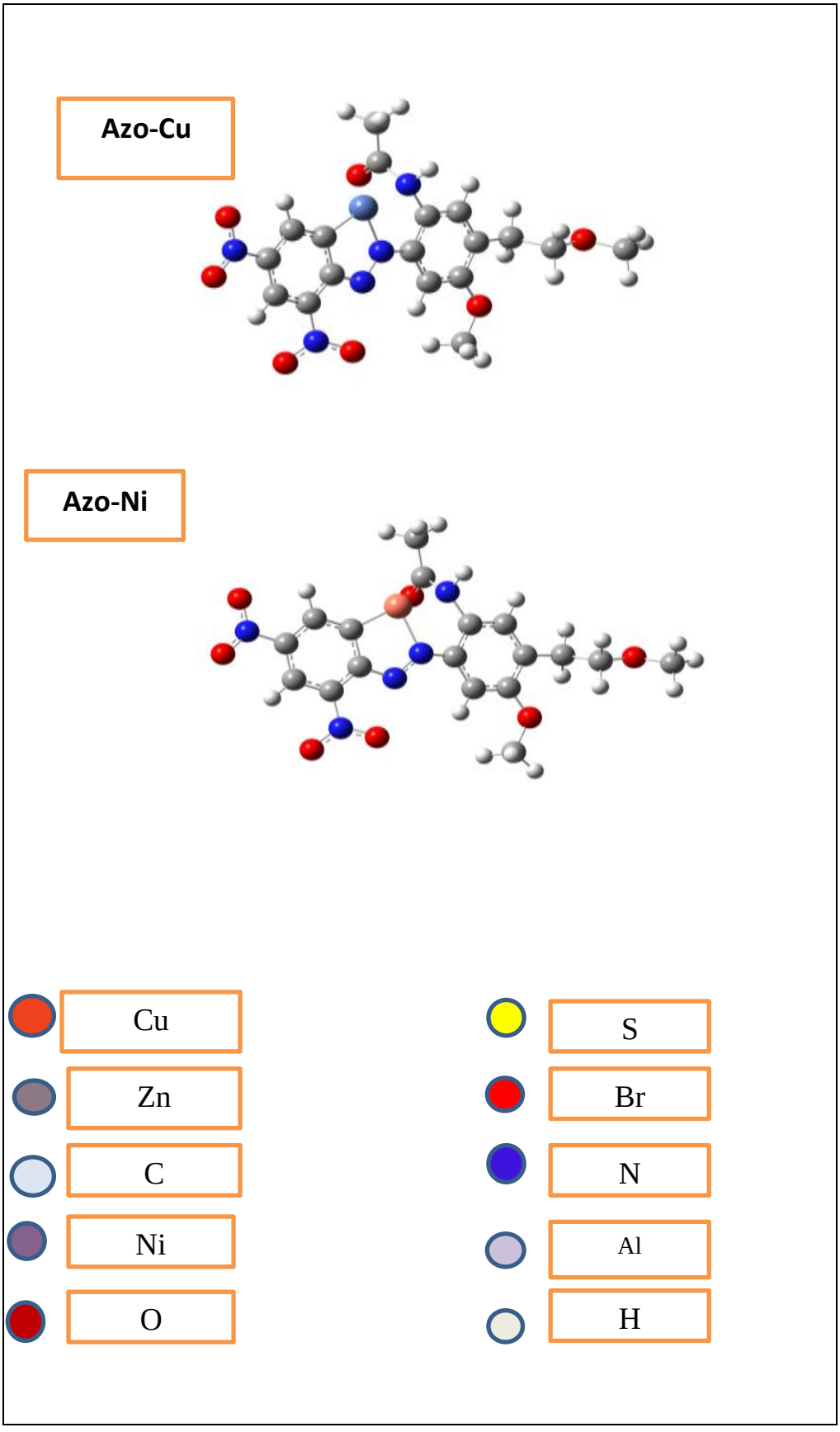

Figure (3-2): The optimized azo dye and azo doping with (Si, S, Ti , Al, Zn, Cu, Ni) atoms Nanostructures.

3-4 HOMO, LUMO and Energy Gap for Azo and Azo Doping Dye

The HOMO, LUMO, and E_g for azo and azo doped with (Si, Ti, S, Zn, Al, Cu, Ni) atoms have been discussed.

HOMOs ,LUMOs, and The HOMO-LUMO gap of the nanostructures plays a significant role in the efficiency of electron injection and the regeneration driving force. For high electron injection efficiency (high charge transfer) the HOMO level of the dye must be very near to and less than the redox potential of the $I^{`}/I_3^{`}$ electrolyte (−4.8 eV), while the LUMO level must be greater than the conduction band minimum CBM of TiO_2 (−4.3 eV). The HOMOs and LUMOs for all the nanostructures, the CBM of TiO_2 and $I^{`}/I_3^{`}$ redox potential levels are shown in Fig. (3-2). Therefore, all the energy levels of the nanostructures except (azo-Al) satisfy the requirement of DSSCs [102] .This figure illustrates that the LUMOs of all nanostructures except (azo- Al) is higher than the CBM of TiO_2 and the redox energy level of $I^{`}/I_3^{`}$ electrolyte is greater than HOMO levels. From Fig (3.2) the azo-Ti have the LUMO level (-3.887 eV) which is higher than the CBM of TiO_2 and HOMO (-5.212 eV) is lower than the redox potential level of $I^{`}/I_3^{`}$ electrolyte, which is a confirmation that the electrons will be injected into the electrode effectively.

The electron transfer from HOMO to LUMO, and the charge separation of carriers, which modify the recombination rate of the electron-hole, are important two factors impacting the DSSC efficiency. Fig.(3-3) shows the configuration HOMO and LUMO orbital nanostructures and their spatial charge separation. From this figure ,Can be noted that the HOMOs of azo-Si, azo-S, and azo-Cu nanostructures are localized on the part which contains the Si, S, and Cu atoms, respectively where the Si, S, and Cu atoms are contributed as the donor. Meanwhile, the LUMOs are restricted on another side of these nanostructures. Therefore, there is apparent

spatial charge separation, as a consequence, the electron-hole recombination in these nanostructures is slow, which is very favorable to the efficiency of conversion for DSSC. On the other hand, the other nanostructures clearly do not show actual spatial charges separations, on which the LUMOs and HOMOs orbitals are constrained on the similar part of the nanostructures. Thus, the spatial charge separations are minor. Hence, the recombination rate of electron-hole will be fast and the DSSCs efficiency is low. These results indicate that azo-Si, azo-S and azo-Cu are favorable sensitizers for DSSCs.

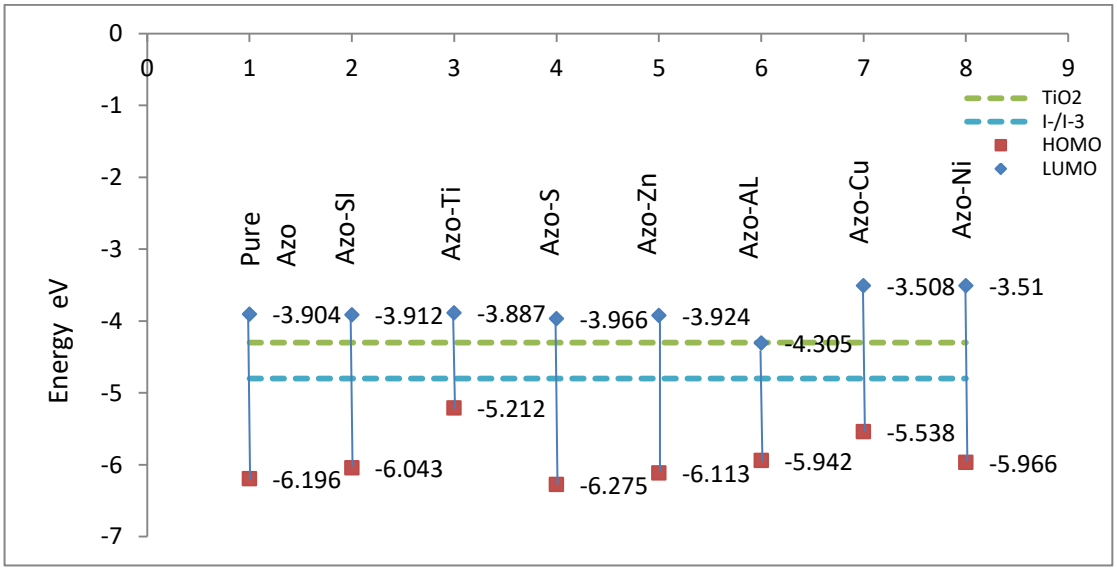

Figure (3. 3): The HOMOs and LUMOs energy levels for all the nanostructures, the CBM of Tio_2, and $I^{`}/I_3^{`}$ redox potential levels.

The calculation shows the energy gap of the azo dye equal 2.292 eV, but when added one of the following atoms (Si, Ti, S, Zn, Al, Cu, Ni) it showed a direct effect on the values of the energy gap, as shown in Table (3-1), especially when adding titanium atom, the HOMO and LUMO levels of azo-Ti are higher than azo dye, therefore, the energy gap decreased to (1.325 eV), which means that the energy bundles converge and the number of transfer electrons will be increased. The electron

transfer depends on the value of the energy gap, all values of energy gaps (1.325-2.456) eV for nanostructures are suitable for electron transforms.

Nanostructures	HOMO	LUMO
Pure Azo	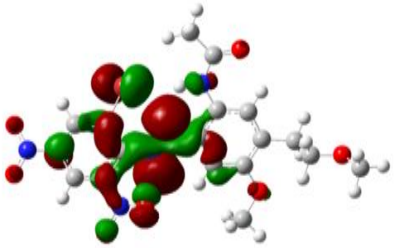	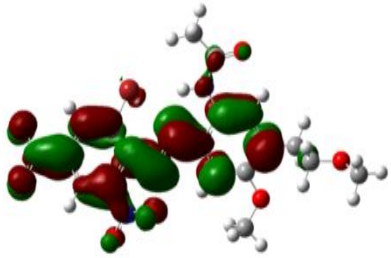
Azo-Si	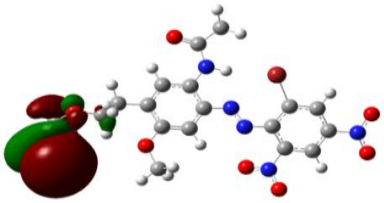	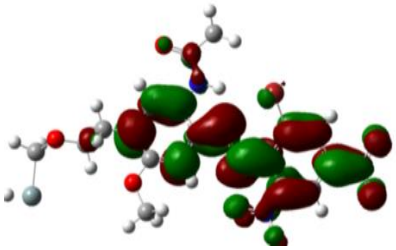
Azo- Ti	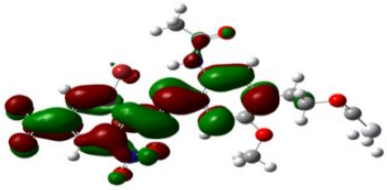	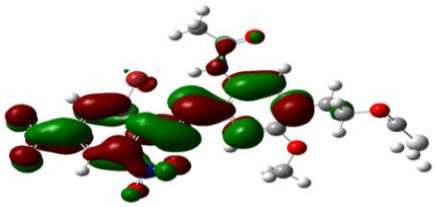
Azo-S	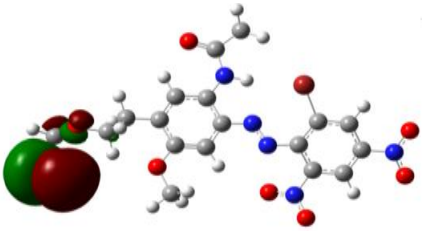	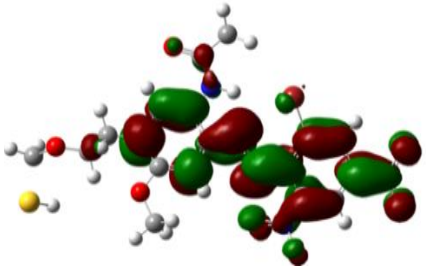

Azo-Zn	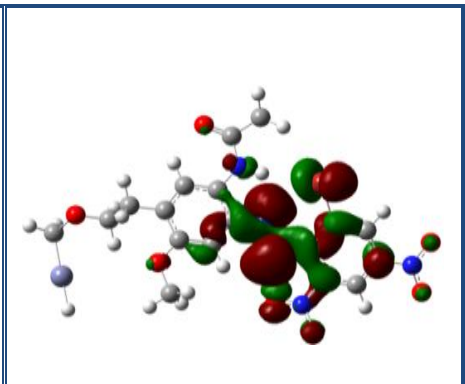	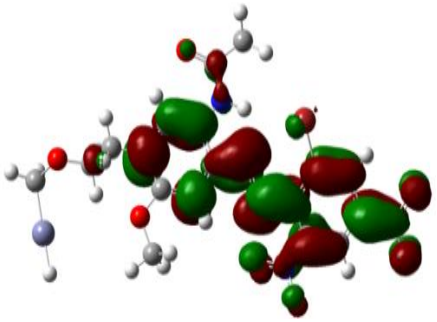
Azo-Al	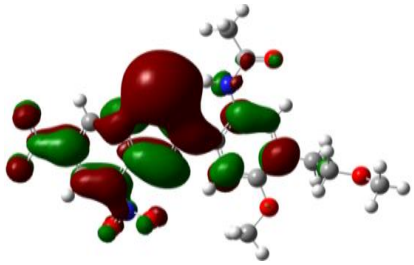	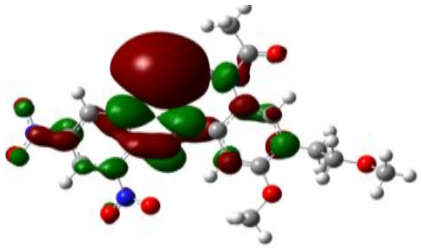
Azo-Cu	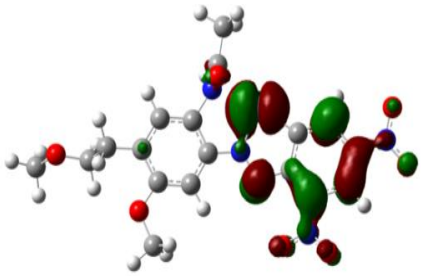	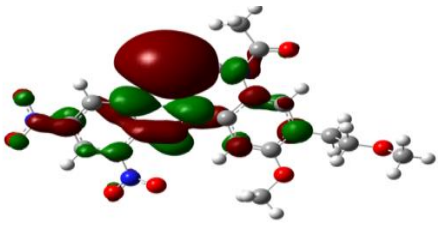
Azo-Ni	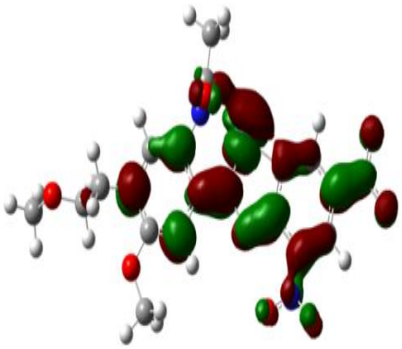	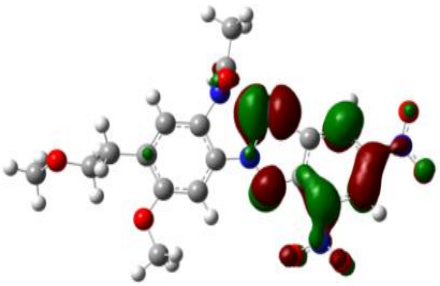

Figure (3.4): The HOMOs and LUMOs for nanostructures.

Table (3. 1): The HOMO LUMO and energy gap of nanostructures.

Nanostructures	HOMO (eV)	LUMO (eV)	Eg= LUMO- HOMO (eV)
Pure Azo	-6.197	-3.905	2.292
Azo-Si	-6.043	-3.912	2.131
Azo-Ti	-5.212	-3.887	1.325
Azo-S	-6.275	-3.966	2.309
Azo-Zn	-6.113	-3.924	2.189
Azo-Al	-5.942	-4.305	1.637
Azo-Cu	-5.538	-3.508	2.030
Azo-Ni	-5.966	-3.510	2.456

3-5 Absorption Spectra and Light Harvesting Efficiency for Azo Dye and Azo Doping

The absorption spectrum and light-harvesting efficiency are the important parameters for DSSCs.The absorption spectra of nanostructures are shown in Fig.(3.4). It is clear from the spectra that adding (Si, Ti, S, Zn, Al, Cu, Ni) atoms produced the shift of spectrum for azo dye toward the visible region for most nanostructures.

All nanostructures have good absorbance in the visible region except the azo-Ni nanostructure. The maximum wavelength (λ_{max}) corresponding to maximum intensity,oscillation strength (f) and light-harvesting efficiency (LHE) are presented in Table (3.2). The pure azo, azo-S, and azo-Zn nanostructures have two peaks. The pure azo , azo-Zn, and azo-Al nanostructures can be used in light-harvesting systems but are not very favorable for DSSCs.

The most favorable nanostructure for DSSCs is azo-S because it has good light-harvesting efficiency, charge spatial separation, appropriate HOMO and LUMO, and suitable driving force, so that, it has satisfied all requirements for a DSSCs desired system [102].

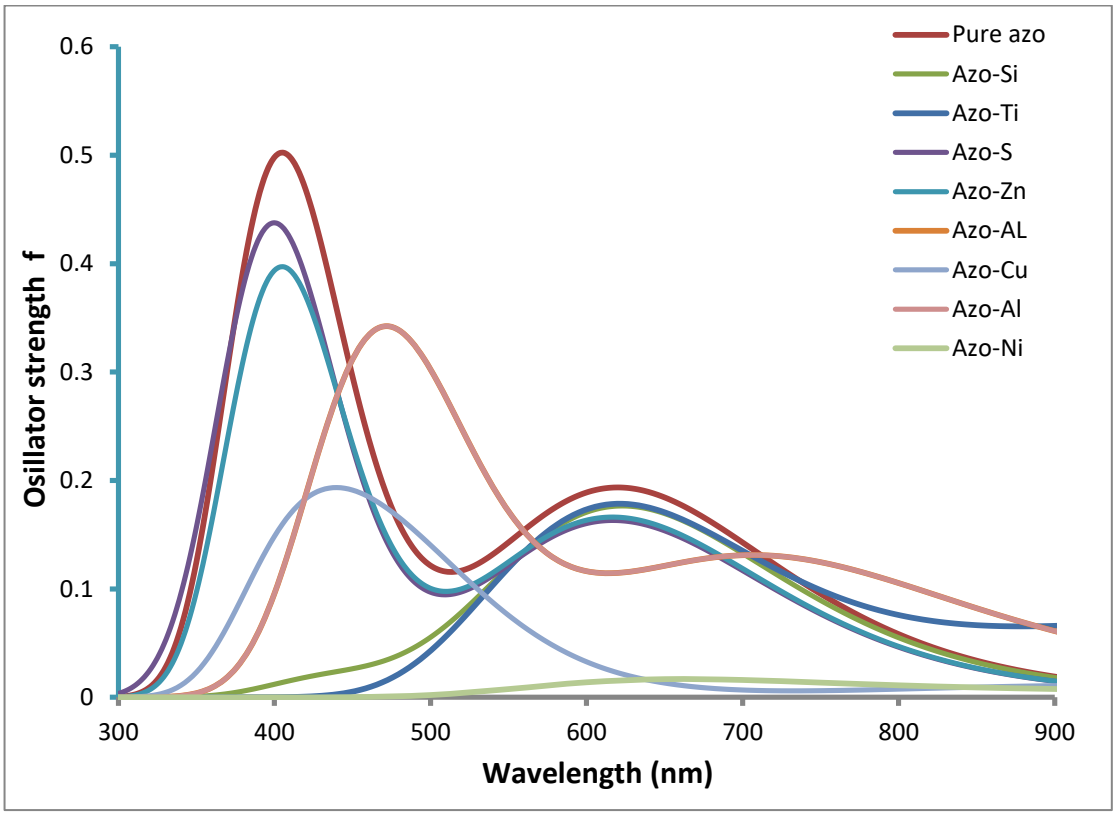

Figure (3.5): UV-Vis. for all the nanostructures.

Table (3. 2): λmax, f, LHE for nanostructures.

Nanostructures	λ_{max} nm	F	LHE %
Pure azo	406	0.502	68.522
	618.8	0.193	35.879
Azo-Si	621.6	0.176	33.319
Azo- Ti	623	0.178	33.625
Azo-S	399.2	0.437	63.44
	617.6	0.163	31.293
Azo-Zn	406	0.397	59.913
	616	0.1662	31.797
Azo-Al	472	0.342	54.501
Azo-Cu	440	0.193	35.879
Azo-Ni	650	0.0167	3.772

3-6 Single walled carbon nanotubes.

In this section we will study the properties of different type of single walled carbon nanotubes, then, study the effect of these nanotubes on the

azo dye as a DSSC .This properties contain the geometrical, electronic and optical properties of different types of single walled carbon nanotubes (SWCNT). Geometrical properties includes bond length and angle between atoms. Electronic properties are molecular orbitals energy, band gap and open voltaic circuits (Voc). Optical properties represented by ultraviolet-visible spectrum (UV-Vis.). After investigating all properties of SWCNT , connect them with Azo organic dye.

3-7 Computational Method for SWCNTs.

SWCNTs of different diameters and lengths (2,2,10), (2,2,14), and (3,3,8) are constructed by Gaussian 09 program as shown in Fig.(3. 5). The UV-Vis spectrum, efficiency, energy gap, maximum wavelength the harmonic oscillation of the greatest wavelength, the highest energy level occupied by electrons and the lowest unoccupied energy level are investigated.

System	Geometrical Structure
(2,2,10)	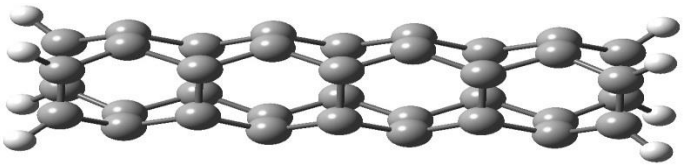
(2,2,14)	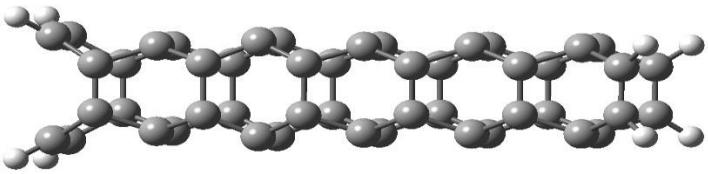

(3,3,8)	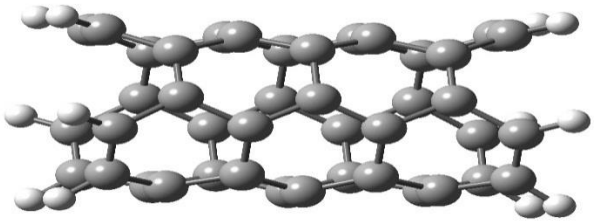

Figure (3.6): Single walled Carbon nanotubes of different diameters and lengths (2,2,10), (2,2,14) and (3,3,8).

3-8 HOMOs, LUMOs and Energy Gaps for SWCNTs.

In the present section, study the effect of nanotubes length on molecular orbital's energy and energy gap. Table (3. 3) listed the values of the higher occupied molecular orbitals (HOMO) and lower unoccupied molecular orbital (LUMO), and the energy gap measured in eV unit.

Table (3.3): Listed values of HOMOs, LUMOs, and energy gap in eV for SWCNTs.

SWCNT	HOMO(ev)	LUMO(ev)	Eg (ev)
(3, 3,8)	**-4.3483**	**-2.3292**	**2.019**
(2, 2,10)	**-4.8283**	**-2.5937**	**2.234**
(2, 2,14)	**-4.8245**	**-2.8952**	**1.929**

Results in Table (3.3) show that the nanotube length and charity have a direct effect on molecular orbitals energy, and the shift in HOMO and LUMO levels plays an essential effect in the electron transfer process. The values of the energy gap show that all carbon nanotubes have a semiconductor nature. To complete the regeneration and recombination process, the nanotubes should satisfy two important conditions, first, all LUMO levels should be arranged above the conduction band minimum CBM of TiO_2 (−4.3eV). secondly, the HOMO level should be arranged below the oxidation potential of the iodine/tri-iodine electrolyte (−4.8eV).

The result in Table (3.3) concludes that only the (2,2,10) and (2,2,14) satisfied the conditions of the regeneration and recombination process, and they can inject an electron in the CBM of (TiO_2).

Figuer(3.6)shows the distribution of charge in orbitals of HOMO and LUMO levels for nanotubes. from this figure, we note that the HOMOs of (2,2,10) and (2,2,14) nanotubes are localized in the central part. Meanwhile, the LUMOs are distributed in all parts of nanotubes. Therefore, there is apparent spatial charge separation, as a consequence, the electron-hole recombination in these nanotubes is slow, which is very favorable to the efficiency of conversion for DSSC. Conversely, the (3,3,8) nanotubes do not appear in actual spatial charge distribution, on which the LUMOs and HOMOs are distributed on a similar part of the nanotubes. These results refer to (2,2,10) and (2,2,14) nanotubes are favorable sensitizers for DSSC.

Nanostructures	**HOMO**	**LUMO**
(3, 3,8)	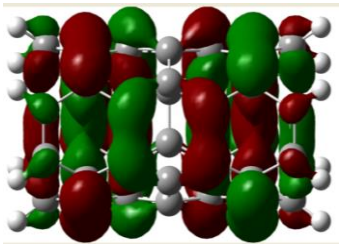	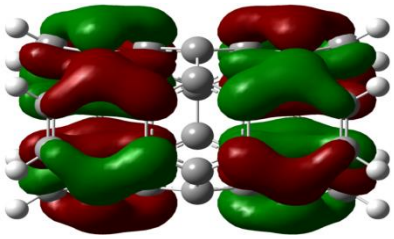
(2, 2,10)	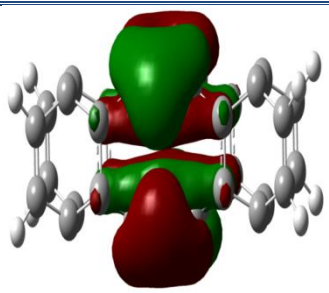	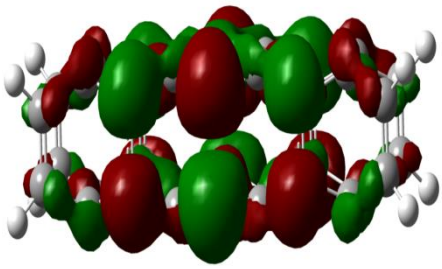

(2, 2,14)	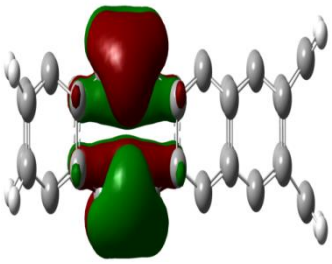	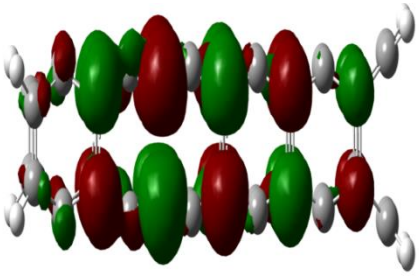

Figure (3.7): HOMOs and LUMOs for the nanotubes.

Also, Figure (3.6) indicates that the electron charge density distribution was increased with an increase in the length and charity. Meanwhile, the distribution becomes more symmetry when the length and charity increase.

Open voltaic circuits can be computed from equation (2-36). V_{OC} property is presented in Table (3.4). Result shows that the nanotube length has had a direct effect on the V_{OC} property. By increasing tube length, the Voc property has being decreased, and it can be arranging in the order (3,3,8) > (2,2,10) > (2,2,14).

Table (3.4): Listed values of (V_{oc})

Nanostructures	V_{oc} Volt
(3, 3,8)	**1.970**
(2, 2,10)	**1.706**
(2, 2,14)	**1.404**

3-9 UV-Visible for SWCNTs.

TD-DFT method was used to compute the oscillation strength f and light harvesting efficiency for all nanotubes understudy. Table (3. 5) indicates that the charity and length of nanotube had a direct effect on LHE and f.

In the case (2,2,10) and (2,2,14) SWCNTs structures, results show that f was decreasing with increased nanotube length from 10 to14 nm because of the symmetry of the nanotube edge. The sample (3, 3,8) had high f compared with other samples. LHE calculations show that (3,3,8) SWCNT has high light harvesting efficiency compared with other structures because it has high oscillation strength values.

Table (3.5): present the values of $\lambda_{(max)}$, f, and LHE for nanotubes

Nanostructures	**λ_{max} nm**	**F**	**LHE %**
(2, 2, 10)	**470**	**0.04**	**8.79**
(2, 2, 14)	**886.45**	**0.003**	**0.688**
(3, 3, 8)	**505.45**	**0.21**	**38.34**

3-10 SWCNT and Azo Dye

In this section of the present work, we selected the structure (3, 3, 8) SWCNT to connected it with azo dye to enhance the electronic and optical properties. Three structures of carbon nanotubes were taken and they are linked with a dye that is impregnated with Cu atoms and the difference is in the binding site, Fig. (3-7) represents the three models. The first structures shows the bonding of the metal atom to the a carbon atom of the nanotube and a carbon atom of the dye. The second model represents the bonding of the metal atom to two carbon atoms of the nanotube and a carbon atom with the dye, while the third structures represents the bonding of the metal atom with the dye nitrogen atom, as shown in Figure (3.7). Table (3.6) listeds the values of molecular orbitals energy and energy gap. Table (3.6) indicates that sample (A) satisfied the condition of the regeneration and recombination process and it could inject the electrons into the TiO_2 electrode. Sample (B) and (C) satisfied

one condition only from the two condition of formation DSSC that is LUMO distribution above CBM(TiO_2), in another hand, it can generate electrons. Meanwhile, the HOMO level was population above $\frac{I^{`}}{I_3^{`}}$ electrolyte, so samples (A) and (C) cannot have the ability to recombination electrons in the electrolyte solution. The above results involve that's, sample (A) was more suitable for application in the DSSCs field. The result of the energy gap shows that all samples have a semiconductor nature.

Sample	optimizations structures
A	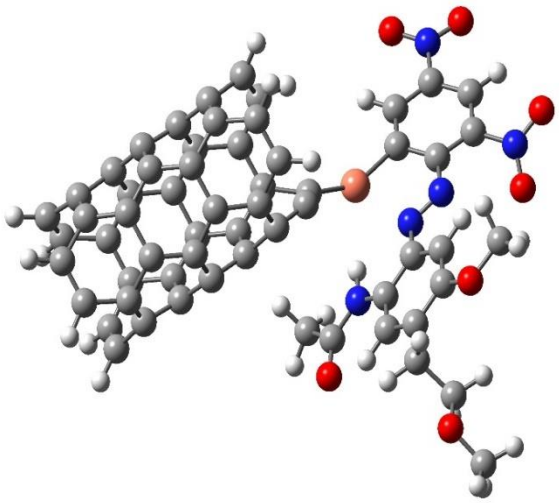
B	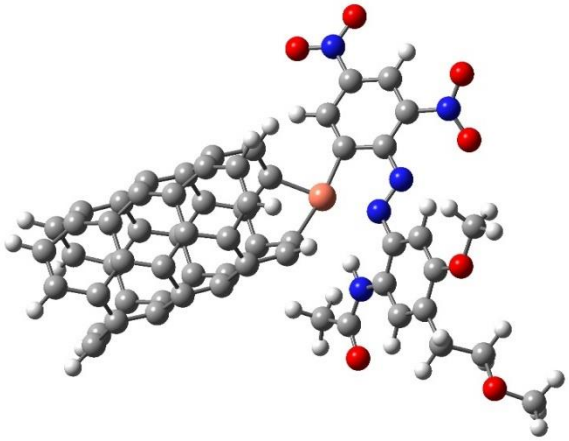

C	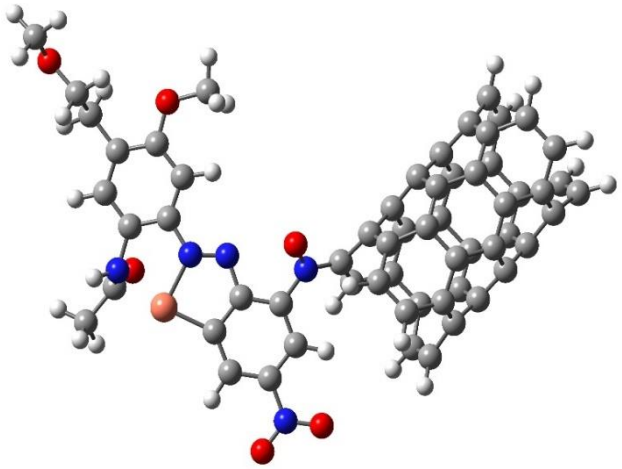

Figure (3.8): Nanocomposites after geometrical optimizations.

Table (3.6): Listes values of HOMOs, LUMOs, and energy gap for nano-composites

Sample	HOMO (eV)	LUMO (eV)	E_g (eV)
A	**-5.15921**	**-3.78233**	**1.376877**
B	**-4.58533**	**-4.09063**	**0.494696**
C	**-4.34369**	**-3.21716**	**1.126535**

Figure (3.8) illustrated the electron charge density distribution generated by the Gaussian view 5.0 program. Electron charge density is one of the important tools that indicate the most stable electron charge surrounding the atoms constituting the nanocomposite. From figure(3.8 A), the results indicate that the most charge density surrounding SWCNT is clear in the HOMO. On the opposite, the charge density distribution indicates that most LUMO overlaps the edge of azo dye. Fig.(3.8) (B and C), have the same distribution of sample (A) but differ in the charge concentration.

Sample	HOMO	LUMO
A	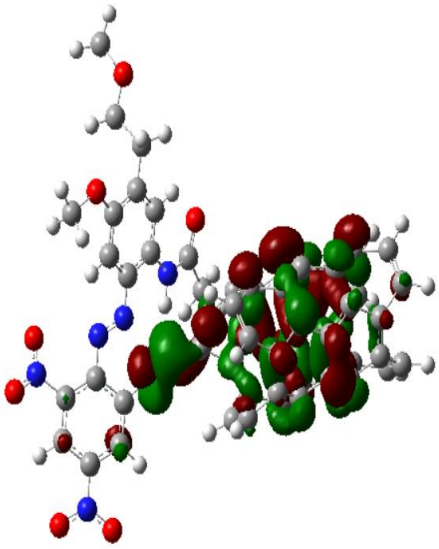	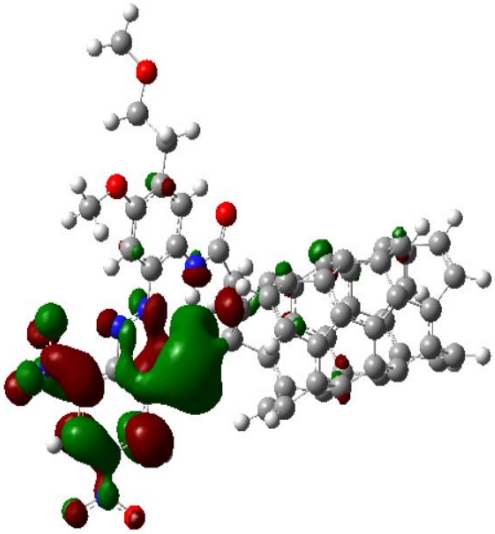
B	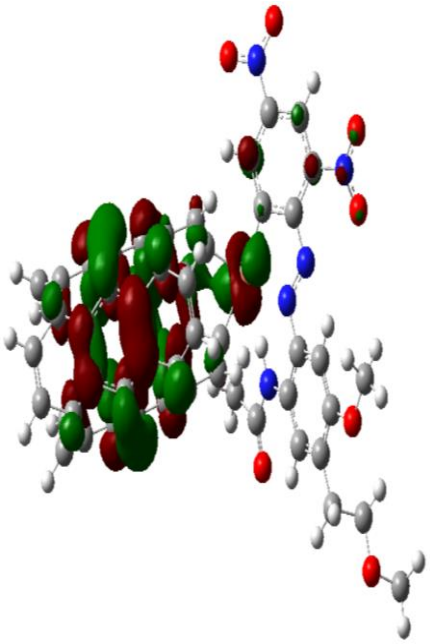	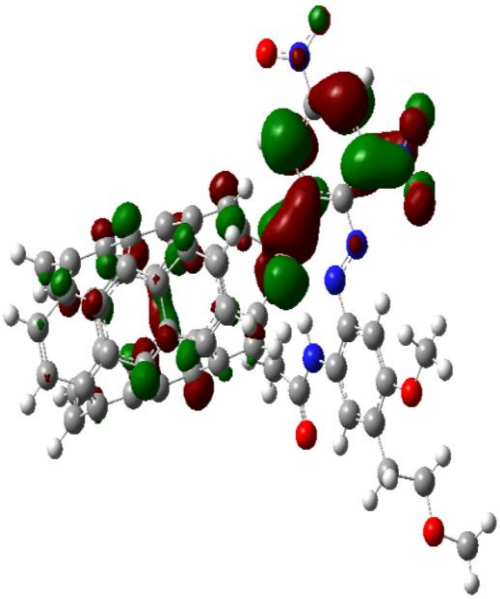

C	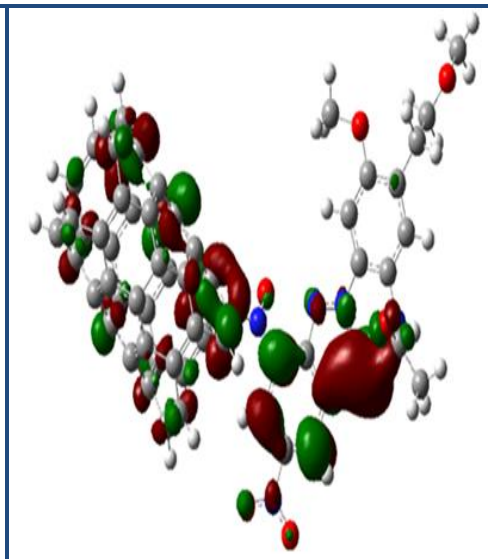	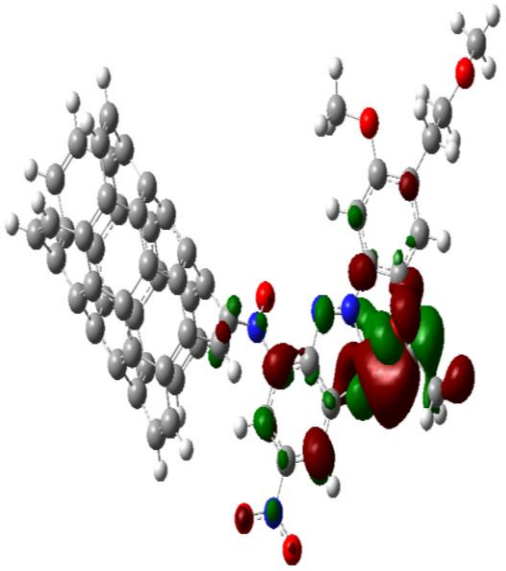

Figure (3.9): HOMOs and LUMOs for the nanocomposites.

3-11 UV-Visible spectrum and open voltaic circuit for Nano-composites

Time dependent-density functional theory TD-DFT calculation was used to compute the maximum wavelength of absorption, oscillation strength, and light harvesting efficiency. UV-Visible spectrum was an important tool to determine the type of shift in electromagnetic radiation. Oscillation strength considers an important parameter for computing LHE and it corresponds maximum wavelength of absorption. Table (3.7) listes the value of the wavelength of absorption, oscillation strength, LHE, and open voltaic circuit .The results show that sample (A) is absorbing in the near-infrared region of electromagnetic radiation. Samples (B) and (C) are absorbed in mid and far-infrared regions of electromagnetic radiation. From above results conclude that sample a was more suitable for absorption in the near-infrared region of electromagnetic radiation compared with the two another samples. LHE calculations show that sample (a) has a high ability to harvest light compared with another sample. V_{oc} results show that sample (a and c) can generate voltaic with

the limitation of organic solar cell device, on the other hand, sample (b) have a low ability to generate gain voltaic. Fig. (3-9) represents the curve of the UV-Visible spectrum for the nanocomposite under study compute by the TD-DFT method.

Table (3.7): Listed values of λ_{max}, f, and LHE for Nano-composites

System	λ_{max} nm	F	LHE %	V_{oc} Volt
A	**987.12**	**0.0542**	**11.7**	**0.21**
B	**1326.73**	**0.02**	**4.50**	**0.09**
C	**1742.58**	**0.0001**	**0.02**	**0.78**

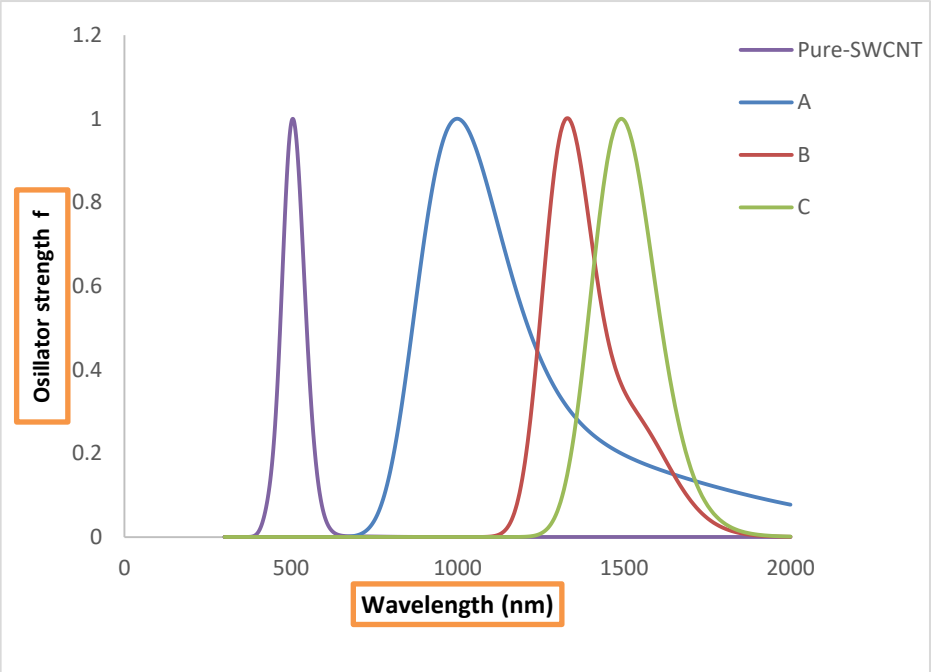

Figure (3.10): The UV-Visible spectrum for nanocomposite.

Chapter four

Conclusions and Future Works

4-1 Conclusions

The geometrical optimizations and electronic properties of azo dye and the effect of doping with (Si, Ti, S, Zn, Al, Cu, Ni) atoms are investigated at the B3LYP/6-31G level, from the result one com conclude that:

1- The HOMOs and LUMOs energy levels of all nanostructures except (azo-Al) satisfy the requirements of DSSCs with the TiO_2 electrode and $I^`/I_3^`$ electrolyte.

2- Azo-Si, azo-S and azo-Cu exhibit spatial charge separation which makes these three nanostructures favorable for sensitizer of DSSC.

3- The results of the optical absorption spectra and light-harvesting efficiency demonstrate that the optical absorptions of azo dye are affected by doping atoms and the nanostructures. (azo-Zn, azo-S, and azo-Al) have an improvement in the visible region, indicating that they are capable to be contenders for use as harvesting materials.

4- Azo-S nanostructure has respectable light-harvesting efficiency, charge spatial separation, appropriate HOMO and LUMO, and appropriate driving force. Therefore, azo-S is a favorable candidate as a sensitizer of DSSCs. These results give guidance for the design of the solar energy harvest materials and enhanced efficient sensitizer of DSSCs.

5- The length and charity of SWCNT play an important role in the change of electronic and optical properties.

6- All the pure SWCNT absorbed in the visible range of electromagnetic radiation.

7- The position of link Cu-doped azo dye with SWCNT effects on regeneration and recombination process.
8- The nanocomposites built from Cu-doped azo and SWCNT are more suitable for solar cell application.

4-2 Future work

1- Investigations the effect of doping azo dye by others atoms in the photosensitizers properties.
2- Building new nanocomposites from SWCNT and others dyes such as curcumin, pahthalocyanine dyes to study their photosensitizer properties.
3- Studying the effect of replacement the SWCNT by graphene quantum dot in the DSSCs.

References

[1] Wang Z. L., 2019" Entropy theory of distributed energy for internet of things *Nano Energy*" , **58** 669–72.

[2] Abdalla A.N., Nazir M.S., Tao H., Cao S., Ji R., Jiang M. and Yao L., 2021, "Integration of energy storage system and renewable energy sources based on artificial intelligence: An overview", *Journal of Energy Storage*, **40** 102811.

[3] Huang X. L., Wang Y.X., Chou S.L., Dou S. X. and Wang Z. M., 2021, "Materials engineering for adsorption and catalysis in room-temperature Na–S batteries", *Energy & Environmental Science*, **14** 3757–95.

[4] Boriskina S. V., Green M. A., Catchpole K., Yablonovitch E., Beard M.C., Okada Y., Lany S., Gershon T., Zakutayev A. and Tahersima M. H., 2016, "Roadmap on optical energy conversion" *Journal of Optics* **,18** 73004.

[5] Singh S.K., Kaushik S.C., Tyagi V.V. and Tyagi S. K., 2021, "Comparative Performance and parametric study of solar still: A review", *Sustainable Energy Technologies and Assessments*, **47** 101541.

[6] Thompson R. C., Crowe T.P., and Hawkins S.J., 2002, "Rocky intertidal communities: past environmental changes, present status and predictions for the next 25 years", *Environmental conservation*, **29** 168–91.

[7] Hayat M. B., Ali D., Monyake K. C., Alagha L. and Ahmed N., 2019, "Solar energy—A look into power generation, challenges, and a solar-powered future", *International Journal of Energy*

Research, **43** 1049–67.

[8] Ahmad L., Khordehgah N., Malinauskaite J. and Jouhara H., 2020, "Recent advances and applications of solar photovoltaics and thermal technologies", *Energy* , **207** 118254.

[9] Mohammed S.A., Mohammed O.A.and Fathi M.G., 2020, "Statistical model of forecasting indicators in one area of sustainable development ", *Periodicals of Engineering and Natural Sciences* , **8** 455–63.

[10] Edensor T., 2017, *"From light to dark Daylight, illumination, and gloom*", **2**88.

[11] Ganesan S., Muthuraaman B., Mathew V., Madhavan J., Maruthamuthu P.and Suthanthiraraj S.A., 2008, "Performance of a new polymer electrolyte incorporated with diphenylamine in nanocrystalline dye-sensitized solar cell", *Solar Energy Materials and Solar Cells* , **92** 1718–22.

[12] Gao L., 2017, "Flexible device applications of 2D semiconductors", *Small* , **13** 1603994.

[13] Adedokun O., Titilope K., and Awodugba A.O., 2016, "Review on natural dye-sensitized solar cells (DSSCs) International Journal of Engineering Technologies", **2** 3441.

[14] Ellmer K. and Bikowski A., 2016, "Intrinsic and extrinsic doping of ZnO and ZnO alloys", *Journal of Physics D: Applied Physics*, **49** 413002.

[15] Chen F., Xia J. and Tao N., 2009, "Ionic screening of charged-impurity scattering in graphene Nano letters", **9** 16215.

[16] Wells A., F., 1984, "Structural Inorganic Chemistry 5th edition p 1277 Oxford Science Publications", **019**8553706.

[17] Inorganic Chemistry., Holleman Wiberg., John Wiley. and Sons, 2001, **8**44.

[18] Ardarelli F., 2008, "Materials handbook,concise desktop reference 2nd ed London: Springer", 158163.

[19] Steudel R., Eckert.B., 2003, "Solid Sulfur Allotropes Sulfur Allotropes" , *Topics in Current Chemistry*, **23**0 180.

[20] García O., Antonio J., Ballabrera P., Emili G., Ladona. and Antonio T., "A global renewable mix with proven technologies and common materials", *Energy Policy*, **41** 2012 561.

[21] Thiemann M., 2018, "Complete electrodynamics of a BCS superconductor with μeV energy scales: Microwave spectroscopy on titanium at mK temperatures", **9**7 21

[22] Pfirrmann, S., Limber C., Herwig C., Stößer R., Ziemer B., 2009, "A Dinuclear Nickel(I) Dinitrogen Complex and its Reduction in Single-Electron Steps", *Angewandte Chemie International Edition*, **33**5761.

[23] Chu J. and Sher A., 2008, "Physics and properties of narrow gap semiconductors", Springer , **987** 387 747.

[24] Ragoussi M.E. and Torres T., 2015, "New generation solar cells: concepts trends and perspectives", *Chemical Communications*, **51** 395772.

[25] Mishra D. R., 2015, "Some breakthroughs in nanoelectronics in the last decade", *International Journal of Engineering Research and General Science*", **3** 1340 57.

[26] Wang Z, Li. C. and Domen K., 2019, "Recent developments in heterogeneous photocatalysts for solar-driven overall water splitting", *Chemical Society Reviews* ,**48** 2109 25.

[27] Renn O. and Marshall J. P., 2016, "Coal, nuclear and renewable energy policies in Germany: From the 1950s to the Energiewende", *Energy Policy*, **99** 224 32.

[28] Jošt M., Kegelmann L., Korte L. and Albrecht S., 2020, "Monolithic perovskite tandem solar cells a review of the present status and advanced characterization methods toward 30% efficiency", *Advanced Energy Materials*, **10** 1904102.

[29] Baran D., Ashraf R., S, Hanifi D. A., Abdelsamie M., Gasparini N., Röhr J. A., Holliday S., Wadsworth A., Lockett S. and Neophytou M., 2017, "Reducing the efficiency–stability–cost gap of organic photovoltaics with highly efficient and stable small molecule acceptor ternary solar cells", *Nature materials*, **16** 3639.

[30] Kamal M. and Rizza G., 2019, "Design for metal additive manufacturing for aerospace applications" *Additive manufacturing for the aerospace industry Elsevier*, **67** 86.

[31] Saito M., Moto K., Nishida T., Suemasu T. and Toko K., 2019, "High-electron-mobility (370 cm2/Vs) polycrystalline Ge on an insulator formed by As-doped solid-phase crystallization", *Scientific Reports*, **9** 1 6.

[32] Buchovska I., Dropka N., Kayser S. and Kiessling F. M., 2019, "The influence of travelling magnetic field on phosphorus distribution in n-type multi-crystalline silicon", *Journal of Crystal Growth*", **507** 299 306.

[33] Ding D., Lu. G., Li. Z., Zhang Y., and Shen W., 2019, "High-efficiency n-type silicon PERT bifacial solar cells with selective emitters and poly-Si based passivating contacts", *Solar Energy*, **193** 494501.

[34] De Wolf S., Descoeudres A., Holman Z. C. and Ballif C., 2012, "High-efficiency silicon heterojunction solar cells A review", *green* **2** 7 24.

[35] Kleinstiver B. P., Tsai S. Q., Prew M. S., Nguyen N. T., Welch M. M., Lopez J. M., McCaw Z. R., Aryee M. J. and Joung J. K., 2016 "Genome-wide specificities of CRISPR-Cas Cpf1 nucleases in human cells", *Nature biotechnology,* **34** 869 74.

[36] Tonita E. M, Valdivia C. E. and Hinzer K., 2020, "Study of carrier transport in bifacial silicon heterojunction solar cells under high air mass illumination", *2020 47th IEEE Photovoltaic Specialists Conference,* **465** 9.

[37] Hedayati M. K., Fahr S., Etrich C., Faupel F., Rockstuhl C. and Elbahri M., 2014, "The hybrid concept for realization of an ultra-thin plasmonic metamaterial antireflection coating and plasmonic rainbow", *Nanoscale* **6** 6037 45.

[38] Shanmugam N., Pugazhendhi R., Madurai Elavarasan R., Kasiviswanathan P. and Das N., 2020, "Anti-reflective coating materials: a holistic review from PV perspective", *Energies* **13** 2631.

[39] Li. H., Zuo. C., Scully A. D., Angmo D., Yang J. and Gao M., 2020, "Recent progress towards roll-to-roll manufacturing of perovskite solar cells using slot-die processing", *Flexible and Printed Electronics*, **5** 14006.

[40] Riede M., Spoltore D. and Leo. K., 2021, "Organic solar cells—the path to commercial success", *Advanced Energy Materials*, **11** 2002653.

[41] Oseni S. O. and Mola G. T., 2017, "Properties of functional layers in inverted thin film organic solar cells" *Solar Energy Materials and Solar Cells* ", **160** 241 56.

[42] Yu Y., Meng B., Jäkle F., Liu J. and Wang L., 2020, "Molecular acceptors based on a triarylborane core unit for organic solar cells" *Chemistry–A European Journal*, **26** 873 80.

[43] Agrawal N., Ansari M. Z., Majumdar A., Gahlot R. and Khare N., 2016, "Efficient up-scaling of organic solar cells", *Solar Energy Materials and Solar Cells*, **157** 960 5.

[44] Sharma S. and Verma A. S., 2013, "A theoretical study of H2S adsorption on graphene doped with B, Al and Ga", *Physica B: Condensed Matter*, **427** 12 6.

[45] Zhang N., Jiang T., Guo C., Qiao L., Ji. Q., Yin L., Yu L., Murto P. and Xu. X., 2020, "High-performance semitransparent polymer solar cells floating on water: Rational analysis of power generation, water evaporation and algal growth", *Nano Energy* ,**77** 105111.

[46] Rybkovskiy D. V., Koroteev V. O., Impellizzeri A., Vorfolomeeva A. A., Gerasimov E.Y., Okotrub A.V., Chuvilin A., Bulusheva L. G. and Ewels C. P., 2022, "Missing One-Dimensional Red-Phosphorus Chains Encapsulated within Single-Walled Carbon Nanotubes *ACS", nano* **16** 600212.

[47] Yan C., Barlow S., Wang Z., Yan H., Jen A KY., Marder S. R. and

Zhan X., 2018, "Non-fullerene acceptors for organic solar cells" *Nature Reviews Materials*, **3** 1 19.

[48] Shayan M. E .and Ghasemzadeh F., 2020, "Nuclear power plant or solar power plant", *Nuclear Power Plants-The Processes from the Cradle to the Grave* IntechOpen**10.**

[49] Ong K.H., Agileswari R., Maniscalco B., Arnou P., Kumar C. C., Bowers J. W. and Marsadek M.B., 2018, "Review on substrate and molybdenum back contact in CIGS thin film solar cell "*International Journal of Photoenergy*, **49.**

[50] Li X., Gao Z., Zhang D., Tao K., Jia R., Jiang S., Wang B., Ji Z., Jin Z. and Liu X., 2020, "High-efficiency multi-crystalline black silicon solar cells achieved by additive assisted Ag-MACE Solar Energy", **195** 176 84.

[51] Bullock J., Hettick M., Geissbühler J., Ong A. J., Allen T., Sutter Fella C. M., Chen T., Ota H., Schaler E. W. and De Wolf S., 2016, "Efficient silicon solar cells with dopant-free asymmetric heterocontacts", *Nature Energy*, **1** 17.

[52] Hieulle J., Stecker C., Ohmann R., Ono L. K. and Qi. Y., 2018, "Scanning probe microscopy applied to organic–inorganic halide perovskite materials and solar cells", *Small Methods* **, 2** 1700295.

[53] Regimol C. C. and Menon C. S., 2007, "Effect of annealing and γ irradiation on tin phthalocyanine thin films", *Mater. Sci. Poland* , **25** 649–55.

[54] Cataldo S., Salice P., Menna E. and Pignataro B., 2012, "Carbon nanotubes and organic solar cells", *Energy and Environmental Science*, **5** 5919 40.

[55] Ding W. L., Wang D. M., Geng Z. Y., Zhao X. L. and Xu. W. B., 2013, "Density functional theory characterization and verification of high-performance indoline dyes with D–A–π–A architecture for dye-sensitized solar cells", Dyes and pigments 98 125 35.

[56] S. Zhang, X., Yang, Y., Numata .and L., Han, 2013, "Highly efficient dye-sensitized solar cells: progress and future challenges," *Energy and Environmental Science*, **6** 5 1443.

[57] Shalini S., 2016, "Investigation on Tio_2 nanostructures sensitized using kigelia africana and hibiscus sabdariffa for dye sensitized solar cells", **16**46 72.

[58] Day J., Senthilarasu S. and Mallick T. K., 2018, "Improving spectral modification for applications in solar cells A review", *Renewable Energy* ,**132** 186 205.

[59] Gao F., Yang C.L., Wang M.S. and Ma X.G., 2018, "Computational studies on the absorption enhancement of nanocomposites of tetraphenylporphyrin and graphene quantum dot as sensitizers in solar cell", *Journal of materials science*, **53** 5140 50.

[60] Michels L., Richter A., Chellappan R. K., Røst H. I., Behsen A., Wells K. H., Leal L., Santana V., Blawid R. and da Silva G. J., 2021, "Electronic and structural properties of the natural dyes curcumin, bixin and indigo", *RSC advances*, **11** 1416977.

[61] Behera A. K. and Sen A., 2022, "Pyrrole-Best Additional Spacers for Azo Based Dye Sensitized Solar Cells: A Computational Study", *Journal of Photochemistry and Photobiology A Chemistry*, **11** 4146.

[62] Periyasamy K., Sakthivel P., Venkatesh G., Anbarasan P. M., Vennila P., Sheena Mary Y., Kaya S. and Erkan S., 2022, "Synthesis, photophysical, electrochemical, and DFT examinations of two new organic dye molecules based on phenothiazine and dibenzofuran", *Journal of Molecular Modeling*, **28** 1 14.

[63] H.J., Kim, D.J., Kim, S. Karthick, K. Hemalatha, C. J., Raj, S. and Y. Choe,2013, "Curcumin dye extracted from Curcuma longa L. used as sensitizers for efficient dye-sensitized solar cells," *International Journal of electrochemical science*, **8** 6 8320.

[64] Chipot C. and Pohorille A., 2007, "Free energy calculations", Springer, **11**83.

[65] Tomasi J., 1999, "Towards “chemical congruence” of the models in theoretical Chemistry", *International Journal for Philosophy of chemistry*, **5** 79 115.

[66] Keith J. A., Vassilev Galindo V., Cheng B., Chmiela S., Gastegger M., Müller K.R. and Tkatchenko A., 2021, "Combining machine learning and computational chemistry for predictive insights into chemical", systems *Chemical reviews*, **121** 9816 72.

[67] Tuckerman M., 2010, "Statistical mechanics: theory and molecular simulation", *Oxford university press*, **13**57.

[68] Cohen A. J., Mori-Sánchez P. and Yang W., 2012, "Challenges for density functional theory", *Chemical reviews*, **112** 289 320.

[69] Berezin F. A. and Shubin M., 2012, "The Schrödinger Equation", *Springer Science & Business Media*, **11**54.

[70] Lepage G. P., 1997, "How to renormalize the Schrodinger equation", *Nuclear Physics*, **13**5.

[71] Rabinowitz P. H., 1992, "On a class of nonlinear Schrödinger equations", *Zeitschrift Angewandte Mathematik und Physik*, **43** 270 91.

[72] Fibich G., 2015, "*The nonlinear Schrödinger equation*", **192** 12.

[73] Sharma H., Wang Z. and Kramer B., 2022, "Hamiltonian operator inference: Physics-preserving learning of reduced-order models for canonical Hamiltonian systems", *Physica Nonlinear Phenomena*, **431** 133122.

[74] Choukroun Y., Shtern A., Bronstein A. and Kimmel R., 2018, "Hamiltonian operator for spectral shape analysis", *IEEE transactions on visualization and computer graphics*, **26** 1320 31.

[75] Myrvold W. C., 2015, "What is a wavefunction? *Synthese*", **192** 3247 74.

[76] Libisch F., Huang C. and Carter E. A., 2014, "Embedded correlated wavefunction schemes Theory and applications", *Accounts of chemical research*, **47** 2768 75.

[77] Valeev E. F. and Sherrill C. D., 2003, "The diagonal Born–Oppenheimer correction beyond the Hartree–Fock approximation" *The Journal of chemical physics*, **118** 3921 7.

[78] Hanna C. B., Laughlin R. B. and Fetter A. L., 1989, "Quantum mechanics of the fractional-statistics gas Hartree-Fock approximation", *Physical Review*, **40** 8745.

[79] Epperlein F., Schreiber M. and Vojta T., 1997, "Quantum Coulomb glass within a Hartree-Fock approximation", *Physical Review*, **56** 5890.

[80] Schulze H.J., Lejeune A., Cugnon J., Baldo M. and Lombardo U., 1995, "Hypernuclear matter in the Brueckner-Hartree-Fock approximation", *Physics Letters*, **355** 21 6

[81] Obot I B, Macdonald D D and Gasem Z M 2015 Density functional theory (DFT) as a powerful tool for designing new organic corrosion inhibitors Part 1 an overview *Corrosion Science* **99** 1–30

[82] Kirklin S., Saal J. E., Meredig B., Thompson A., Doak J. W., Aykol M., Rühl S. and Wolverton C., 2015, "The Open Quantum Materials Database (OQMD) assessing the accuracy of DFT formation energies ", *npj Computational Materials*, **1** 1 15.

[83] Ireta J., Neugebauer J. and Scheffler M., 2004, "On the accuracy of DFT for describing hydrogen bonds dependence on the bond directionality", *The Journal of Physical Chemistry*, **108** 5692 8.

[84] Burns L. A., Mayagoitia A. V., Sumpter B. G. and Sherrill C. D., 2011, "Density-functional approaches to noncovalent interactions: A comparison of dispersion corrections (DFT-D), exchange-hole dipole moment (XDM) theory, and specialized functionals", *The Journal of Chemical Physics*, **134** 84107.

[85] Schuchardt K. L., Didier B. T., Elsethagen T., Sun L., Gurumoorthi V., Chase J., Li. J. and Windus T. L., 2007, "Basis set exchange: a community database for computational sciences", *Journal of chemical information and modeling*, **47** 1045 52.

[86] Brockherde F., Vogt L., Li. L., Tuckerman M. E., Burke K. and Müller K.R., 2017, "Bypassing the Kohn-Sham equations with machine learning", *Nature communications*, **8** 1 10.

[87] Yu. H. S., Li. S. L. and Truhlar D. G., 2016, "Perspective: Kohn-

Sham density functional theory descending a staircase", *The Journal of chemical physics*, **145** 130901.

[88] Fleming I., 2011, "Molecular orbitals and organic chemical reactions", John Wiley and Sons, **60**9.

[89] Zakutayev A., Woods-Robinson R., Han Y., Zhang H., Khan I., Persson K. and Ablekim T., 2020, "Wide band gap chalcogenide semiconductors", *Chemical Reviews*, **120.**

[90] Tanaka I., Oba F., Tatsumi K., Kunisu M., Nakano M. and Adachi H., 2002, "Theoretical formation energy of oxygen-vacancies in oxides", *Materials Transactions*, **43** 1426 9.

[91] Laricchia G., Van Reeth P., Szluinska M. and Moxom J., 2002, "Total positron-impact ionization and positronium formation from the noble gases", *Journal of Physics B Atomic, Molecular and Optical Physics*, **35** 2525.

[92] Elmi F., Movaghar A. F., Elmi M. M., Alinezhad H. and Nikbakhsh N., 2017, "Application of FT-IR spectroscopy on breast cancer serum analysis", *Spectrochimica Acta Part A Molecular and Biomolecular Spectroscopy*, **187** 87 91.

[93] Djomgoue P. and Njopwouo D., 2013, "FT-IR spectroscopy applied for surface clays characterization", *Journal of Surface Engineered Materials and Advanced Technology* , **3** 275.

[94] Zhou Y. and Tang R.C., 2016, "Modification of curcumin with a reactive UV absorber and its dyeing and functional properties for silk", *Dyes and Pigments*, **134** 203 11.

[95] Miraftab R., Ramezanzadeh B., Bahlakeh G. and Mahdavian M.,

2017, "An advanced approach for fabricating a reduced graphene oxide-AZO dye/polyurethane composite with enhanced ultraviolet (UV) shielding properties Experimental and first-principles QM modeling", *Chemical Engineering Journal*, **321** 159 74.

[96] Erickson C. B., Ankenman B. E. and Sanchez S. M., 2018, "Comparison of Gaussian process modeling software", *European Journal of Operational Research*, **266** 179 92.

[97] Patterson M. A. and Rao A. V., 2014, "A MATLAB software for solving multiple-phase optimal control problems using hp-adaptive Gaussian quadrature collocation methods and sparse nonlinear programming", *ACM Transactions on Mathematical Software* , **41** 1 37.

[98] Allouche A., 2011, "Gabedit A graphical user interface for computational chemistry", softwares *Journal of computational chemistry*, **32** 174 82.

[99] Gong J., Sumathy K., Qiao Q. and Zhou Z., 2017, "Review on dye-sensitized solar cells (DSSCs) Advanced techniques and research trends", *Renewable and Sustainable Energy Reviews*, **68** 234 46.

[100] Karim N. A., Mehmood U., Zahid H. F. and Asif T., 2019, "Nanostructured photoanode and counter electrode materials for efficient Dye-Sensitized Solar Cells ", *Solar Energy*, **185** 165 88.

[101] Al-Seady M. A., Abdul Wahhab N. A., Abbood H. I. and Abduljlil H. M., 2021, "DFT Study of Chemical Adsorption of NO2 Gas on Graphene Nano Material", *Materials Science Forum* Trans Tech Publ, **391** 7

[102] Mohammad R. K., Nowfal S. H., Al-Seady M. A. and Abduljalild H. M., 2022, "Investigation Ability of Single Walled Carbon Nanotubes to Detection Toxic Gases Utilizing DFT Calculations", *Egyptian Journal of Chemistry*, **65** 1 2.